Supplemental material to this article can be found at:
http://jpet.aspetjournals.org/content/suppl/2018/04/10/jpet.118.247767.DC1

1521-0103/365/3/688–699$35.00
THE JOURNAL OF PHARMACOLOGY AND EXPERIMENTAL THERAPEUTICS
Copyright © 2018 by The American Society for Pharmacology and Experimental Therapeutics
https://doi.org/10.1124/jpet.118.247767
J Pharmacol Exp Ther 365:688–699, June 2018

The Journal of PHARMACOLOGY And Experimental Therapeutics

In Vitro–In Vivo Extrapolation of OATP1B-Mediated Drug–Drug Interactions in Cynomolgus Monkey[S]

Ayşe Ufuk, Rachel E. Kosa, Hongying Gao, Yi-An Bi, Sweta Modi, Dana Gates, A. David Rodrigues, Larry M. Tremaine, Manthena V. S. Varma, J. Brian Houston, and Aleksandra Galetin

Centre for Applied Pharmacokinetic Research, School of Health Sciences, University of Manchester, Manchester, United Kingdom (A.U., J.B.H., A.G.); and Pharmacokinetics, Dynamics, and Metabolism (R.E.K., H.G., Y.-A.B., A.D.R., L.M.T., M.V.S.V.) and Research Formulations, Pharmaceutical Sciences (S.M., D.G.), Medicine Design, Pfizer Worldwide R&D, Groton, Connecticut

Received January 9, 2018; accepted April 6, 2018

ABSTRACT

Hepatic organic anion-transporting polypeptides (OATP) 1B1 and 1B3 are clinically relevant transporters associated with significant drug–drug interactions (DDIs) and safety concerns. Given that OATP1Bs in cynomolgus monkey share >90% degree of gene and amino acid sequence homology with human orthologs, we evaluated the in vitro–in vivo translation of OATP1B-mediated DDI risk using this preclinical model. In vitro studies using plated cynomolgus monkey hepatocytes showed active uptake K_m values of 2.0 and 3.9 μM for OATP1B probe substrates, pitavastatin and rosuvastatin, respectively. Rifampicin inhibited pitavastatin and rosuvastatin active uptake in monkey hepatocytes with IC_{50} values of 3.0 and 0.54 μM, respectively, following preincubation with the inhibitor. Intravenous pharmacokinetics of $^2H_4$-pitavastatin and $^2H_6$-rosuvastatin (0.2 mg/kg) and the oral pharmacokinetics of cold probes (2 mg/kg) were studied in cynomolgus monkeys ($n = 4$) without or with coadministration of single oral ascending doses of rifampicin (1, 3, 10, and 30 mg/kg). A rifampicin dose-dependent reduction in i.v. clearance of statins was observed. Additionally, oral pitavastatin and rosuvastatin plasma exposure increased up to 19- and 15-fold at the highest dose of rifampicin, respectively. Use of in vitro IC_{50} obtained following 1 hour preincubation with rifampicin (0.54 μM) predicted correctly the change in mean i.v. clearance and oral exposure of statins as a function of mean unbound maximum plasma concentration of rifampicin. This study demonstrates quantitative translation of in vitro OATP1B IC_{50} to predict DDIs using cynomolgus monkey as a preclinical model and provides further confidence in application of in vitro hepatocyte data for the prediction of clinical OATP1B-mediated DDIs.

Introduction

Drug–drug interactions (DDIs) involving hepatic organic anion-transporting polypeptides (OATPs) are widely recognized as clinically important due to potential serious adverse events associated with them (Giacomini et al., 2010; Yoshida et al., 2012; El-Kattan et al., 2016; Galetin et al., 2017). Therefore, there is a strong need to assess OATP-mediated DDI risk early in candidate identification and drug development. Despite tremendous strides in establishing in vitro tools for assessing transporter role, confidence in quantitative prediction of transporter-mediated DDIs using in vitro data is arguably still low to moderate (Zamek-Gliszczynski et al., 2013; Jones et al., 2015; Yoshida et al., 2017).

Recently, cynomolgus monkey has been increasingly evaluated as a potential animal model for the assessment of OATP1B-mediated DDIs (Shen et al., 2013, 2015; Takahashi et al., 2013, 2016; Chu et al., 2015) due to >90% degree of gene and amino acid sequence homology between cynomolgus monkey and human orthologs for OATP1B uptake transporters (Ebeling et al., 2011; Shen et al., 2013; Takahashi et al., 2013). In addition to clinical drug probes, increasing evaluation of endogenous biomarkers for OATP1B DDIs (e.g., coproporhyrin I, bile acids) has been reported in this preclinical species (Chu et al., 2015; Watanabe et al., 2015; Shen et al., 2016; Thakare et al., 2017). DDIs reported in cynomolgus monkey for statins, including rosuvastatin, pitavastatin, and atorvastatin, showed a good agreement in DDI classification (strong/moderate) relative to those observed in humans

A.U. was supported by a consortium of pharmaceutical companies (Eli Lilly, Pfizer, GlaxoSmithKline) within the Centre for Applied Pharmacokinetic Research at the University of Manchester.
https://doi.org/10.1124/jpet.118.247767.
[S] This article has supplemental material available at jpet.aspetjournals.org.

ABBREVIATIONS: AUC, area under the plasma concentration–time curve; AUCR, ratio of the AUC; BCRP, breast cancer resistance protein; CL_{active}, active uptake clearance; CL_{diff}, passive diffusion clearance; CL_{iv}, i.v. clearance; C_{max}, maximum plasma concentration; DDI, drug–drug interaction; DPBS, Dulbecco's phosphate-buffered saline; F, oral bioavailability; F_a, fraction absorbed; F_g, fraction of drug escaping intestinal extraction; F_h, fraction of drug escaping hepatic extraction; $f_{u,med}$, nonspecific binding in the media; HEK293, human embryonic kidney 293; IVIVE, in vitro–in vivo extrapolation; LC-MS/MS, liquid chromatography–tandem mass spectrometry; MRP2, multidrug resistance protein 2; NTCP, sodium taurocholate cotransporting polypeptide; OATP, organic anion-transporting polypeptide; $t_{1/2}$, half-life; Vd_{ss}, volume of distribution.

Downloaded from jpet.aspetjournals.org at ASPET Journals on April 19, 2024

(summary in Supplemental Table 1). However, direct comparison of hepatic transporter-mediated DDIs between humans and monkeys may be challenging due to species differences in dosing regimen, transporter expression levels, activities, and/or mechanisms involved in drug clearance. For instance, cynomolgus monkey liver expression of OATP1B1 and OAT1B3 was shown to be ~6- to 13-fold higher compared with human liver, respectively (Wang et al., 2015). In the case of OATP2B1 and sodium taurocholate cotransporting polypeptide (NTCP), the protein levels were either ~6-fold greater in human liver or comparable between the two species, respectively (Wang et al., 2015). Nevertheless, an in vitro–in vivo extrapolation (IVIVE) strategy using either static or physiologically-based pharmacokinetic modeling approaches accounting for the species differences could be employed for predicting clinical DDI risk.

Discrepancy in the translation of inhibitory potency (IC_{50} or K_i) to in vivo was reported for OATP inhibitors (Varma et al., 2012; Li et al., 2014; Yoshikado et al., 2017). For example, rifampicin in vitro K_i values were shown to be several fold higher than the in vivo K_i estimated from the clinical DDI data using mechanistic modeling (Varma et al., 2014; Barnett et al., 2017; Yoshikado et al., 2017). In addition, a number of studies demonstrated potentiation of OATP1B inhibition following preincubation with the inhibitor, trend particularly evident for cyclosporine (Amundsen et al., 2010; Gertz et al., 2013; Izumi et al., 2015; Takahashi et al., 2016; Pahwa et al., 2017) and incorporated in the recent Food and Drug Administration DDI guidance document (https://www.fda.gov/downloads/Drugs/Guidances/UCM581965.pdf). Although the clinical DDIs with cyclosporine are well recovered with the IC_{50} obtained following preincubation (Gertz et al., 2013), there is limited understanding of the significance of preincubation in predicting DDIs of other inhibitor drugs. Additionally, recent studies reported substrate dependence in the in vitro inhibition data for OATP1B inhibitors (Noé et al., 2007; Izumi et al., 2013). Due to the gaps in the available clinical DDI data, understanding of the translation of preincubation and substrate-dependent inhibition in vitro phenomena is still ambiguous.

Using cynomolgus monkey as a preclinical model, our goals in the current study are as follows: 1) to evaluate the predictability of OATP1B-mediated DDIs from in vitro inhibition data and 2) to understand the in vivo relevance of the effect of preincubation and substrate dependency in rifampicin inhibition potential measured in vitro. In this study, the in vitro inhibition of transporter-mediated uptake of rosuvastatin and pitavastatin was investigated after incubation of plated cynomolgus monkey primary hepatocytes either with buffer or OATP inhibitors (rifampicin, cyclosporine, and rifamycin SV). Prior to inhibition studies, an uptake kinetic characterization was performed for these two statins. Pitavastatin and rosuvastatin represent extended clearance classification system class 1B and class 3B, respectively, in which OATP-mediated hepatic uptake is the rate-determining step in the systemic clearance in human (Varma et al., 2015, 2017). To allow separate evaluation of inhibitory effect of hepatic versus intestinal disposition, pharmacokinetics of both statins were studied following simultaneous i.v. (stable-labeled) and oral (cold) administration to cynomolgus monkey ($n = 4$ animals) and over a wide rifampicin dose range (1–30 mg/kg). Finally, the extrapolation of rifampicin in vitro inhibition potency data obtained using monkey hepatocytes to the in vivo changes in systemic clearance and plasma (i.v./oral) exposure of statins was evaluated.

Materials and Methods

Chemicals and Reagents. The 3′-phosphoadenosine-5′-phosphosulfate, simvastatin, rifamycin SV, rifampicin, 1-aminobenzotriazole, cyclosporine A, naloxone, and tolbutamide were purchased from Sigma-Aldrich (St. Louis, MO). Deuterium-labeled rifampicin ($^2H_8$-rifampicin) was obtained from ALSACHIM (Illkirch, Graffenstaden, France). Pitavastatin and rosuvastatin were purchased from Sequoia Research Products (Oxford, UK). Deuterium-labeled pitavastatin ($^2H_4$-pitavastatin) and rosuvastatin ($^2H_6$-rosuvastatin) were purchased from Clearsynth (Ontario, Canada). Atorvastatin was purchased from Toronto Research Chemicals (Toronto, Canada). InVitroGro CP hepatocyte medium and Torpedo antibiotic mix were purchased from InVitro GmbH (Frankfurt, Germany). Collagen I–coated 24-well plates were obtained from VWR International (Leicestershire, UK). Cryopreserved cynomolgus monkey hepatocytes (female, pooled lot 10353012) were purchased from In Vitro ADMET Laboratories (Columbia, MD). Bicinchoninic acid protein assay kit was purchased from Life Technologies (Paisley, UK). Dulbecco's phosphate-buffered saline (DPBS) was obtained from Life Technologies. Acetonitrile, water, and ammonium hydroxide were obtained from Fisher Scientific (Fair Lawn, NJ). Methanol was purchased from Fisher Scientific and VWR International.

In Vitro Transport Studies Using Monkey Hepatocytes. Cryopreserved cynomolgus monkey hepatocytes were thawed in prewarmed InVitroGRO CP medium supplemented with torpedo antibiotic mix (2.2% v/v), according to the protocol from InVitro GmbH, and cell viability was determined by trypan blue exclusion method. Hepatocyte suspension was diluted to 0.7×10^6 cells/ml with the prepared InVitroGRO CP medium, and hepatocytes were seeded into collagen I–coated 24-well plates at a density of 350,000 cells/well. Cells were cultured for 4 hours at 37°C and 5% CO_2 in an incubator to allow attachment to the collagen. Cell confluency and monolayer formation were visually assessed before each experiment. Both the hepatic transporter uptake and its inhibition were investigated in plated cynomolgus monkey hepatocytes 4 hours postseeding using rosuvastatin and pitavastatin as probe substrates. Uptake was measured over a range of concentrations (0.1-0.3-1-3-10-30-100 μM) for 30, 60, 90, and 120 seconds at 37°C in triplicate to determine uptake kinetics, as described previously (Ménochet et al., 2012).

Inhibition of rosuvastatin and pitavastatin hepatic uptake by monkey hepatocytes was assessed in triplicate using the OATP inhibitor rifampicin (0.01–100 μM). In addition, inhibition with cyclosporine (0.01–6 μM) and rifamycin SV (0.01–1000 μM) was investigated. Cyclosporine was included as a strong OATP inhibitor with evidence of preincubation effect in human in vitro systems (Gertz et al., 2013; Izumi et al., 2015), whereas rifamycin SV was considered as dual inhibitor of OATPs and NTCP (Bi et al., 2017). Rosuvastatin and pitavastatin concentrations used in the inhibition studies were 1 and 0.3 μM, respectively. The medium was removed after plating, and cell monolayers were rinsed twice with prewarmed DPBS. Effect of preincubation on the inhibition of hepatic uptake transporters in cynomolgus monkey hepatocytes was investigated by the addition of an inhibitor solution (400 μl) on the cell monolayer for 1 hour. In control group, preincubation was performed with DPBS containing 1 mM 1-aminobenzotriazole. Following preincubation, cell monolayers were coincubated with prewarmed DPBS containing the inhibitor and the probe substrate for 3 minutes. This incubation was stopped by the removal of the medium and rinsing of the cell monolayers three times with 800 μl ice-cold DPBS. The cell monolayers were lysed in 200 μl ice-cold deionized water for subsequent liquid chromatography–tandem mass spectrometry (LC-MS/MS) analysis. The in vitro sample preparation and LC-MS/MS analysis

Downloaded from jpet.aspetjournals.org at ASPET Journals on April 19, 2024

are described in Supplemental Material, Section 1. The LC-MS/MS conditions for each individual drug and their corresponding internal standards are detailed in Supplemental Table 2.

In Vitro Data Analysis. Determination of the uptake kinetic parameters, including the affinity constant K_m (μM), the maximum uptake rate V_{max} (pmol/min/10^6 cells), passive diffusion clearance (CL_{diff}; microliters per minute per 10^6 cells), and fraction unbound in the cell fraction of unbound drug in the cell for rosuvastatin and pitavastatin, was performed using the two-compartment mechanistic model in Matlab (2015a) (MathWorks, Natick, MA), as described previously (Ménochet et al., 2012). The active uptake clearance (CL_{active}; μl/min/10^6 cells) was estimated from the V_{max} to K_m ratio. Parameter estimates were corrected for nonspecific binding in the media ($f_{u,med}$), which was calculated from the slope of the linear regression of the unbound substrate concentration extrapolated at $t = 0$ versus the initial media concentration curve. The cellular concentrations were normalized for protein content as measured by the bicinchoninic acid protein assay kit at the end of incubation. Hepatocyte volume was set to 3.9 μl/10^6 cells as in rat (Reinoso et al., 2001); conversion of monkey hepatocyte data expressed per mg protein to M cells was based on the 1:1 relationship between milligram protein and M cells (in-house data).

The data on substrate uptake (expressed as percentage of control) at each inhibitor concentration were used to estimate the IC_{50} (μM) of the inhibitors used. The analysis was performed in GraFit v6.0 (Erithacus Software, Horley, UK) by fitting a nonlinear least squares regression model, as shown in eq. 1 to the experimental data:

$$Substrate\ uptake\ (\%\ control) = \frac{Max - Min}{1 + \left(\frac{I}{IC_{50}}\right)^{s}} + Min \tag{1}$$

where *Max* and *Min* represent the fitted maximum and minimum uninhibited uptake, respectively, I is the inhibitor concentration, corrected for $f_{u,med}$ (0.85, 0.7, and 0.95 for rifampicin, cyclosporine, and rifamycin SV, respectively), and s is the slope factor. To increase the precision of the IC_{50} estimates, the minimum uptake was fixed to the experimental data. In all cases, the experimental data for minimum uptake were within 25% of the estimated value. Statistical analysis of the preincubation effect on IC_{50} was performed using a paired t test, where $p < 0.05$ was considered as statistically significant.

In Vivo Studies in Cynomolgus Monkeys. All procedures performed on these animals were in accordance with regulations and established guidelines, were reviewed and approved by Pfizer Institutional Animal Care and Use Committee, and were conducted at Pfizer (Groton, CT). Male cynomolgus macaque Mauritian monkeys (approximately 6–8.5 years of age) were used for these studies. A crossover study design was employed, in which the same four animals were dosed over a series of five studies, following a minimum 1-week washout period between each study. One exception was the 3 mg/kg rifampicin dose group, in which one of four monkeys was dosed only in that single study. Animals were provided a normal food schedule the day before the study (meals at 8:00 AM and 11:00 AM, with one treat daily) and were allowed free access to water. Animals were housed in metabolism cages during sample collection. On the day of the study, monkeys were fed at approximately 1 and 3 hours postdose and allowed water ad libitum. Rifampicin was administered via oral gavage at 0 (blank vehicle), 1, 3, 10, and 30 mg/kg, at a dose volume of 2 ml/kg in a 0.5% (w/v) methylcellulose (in water) suspension. Rifampicin administration was immediately followed by oral doses of pitavastatin and rosuvastatin at a dose of 2 mg/kg. Approximately 1 hour and 15 minutes following the oral rifampicin administration, $^2H_4$-pitavastatin and $^2H_6$-rosuvastatin were administered via i.v. bolus (cephalic vein), at dose of 0.2 mg/kg, in a dosing volume of 0.2 ml/kg; 2% dimethyl sulfoxide (v/v); and 98% of Tris-buffered saline (pH ~7.7). All i.v. formulations were sterile filtered prior to administration. Serial blood samples were collected via the femoral vein into K_2EDTA tubes prior to dosing and then at 0.083, 0.25, 0.5, 0.75, 1, 2, 3, 5, 6, and 24 hours post i.v. dosing. Blood samples were stored on wet ice prior to being centrifuged to obtain plasma (3000 rpm, 10 minutes at 4°C; Jouan BR4i refrigerated centrifuge). Urine was also collected on wet ice predose and at intervals of 0–6 and 6–24 hours postdose. Due to the potential instability of rifampicin and possible interconversion of lactone and acid forms of pitavastatin or rosuvastatin, each plasma and urine sample was equally divided into two aliquots prior to being stored frozen. The first aliquot was untreated matrix, whereas the second aliquot was added to an equal volume of 0.1 M sodium acetate buffer (pH 4). All urine and plasma samples, treated and untreated, were kept cold during collection, after which they were stored frozen at −20°C. The analysis of $^2H_4$-pitavastatin, $^2H_6$-rosuvastatin, pitavastatin, rosuvastatin, and rifampicin in plasma samples by LC-MS/MS was described in Supplemental Material, Section 2. The analytes were monitored using multiple reaction monitoring with settings listed in Supplemental Table 3.

Pharmacokinetic Analysis and DDI Predictions. Analyst 1.4.2 software (SCIEX, Framingham, MA) was used for LC-MS/MS peak integration of plasma and urine samples. Raw data were imported into Watson LIMS version 7.4 (Thermo Fisher Scientific, Waltham, MA) for standard curve regression and noncompartmental pharmacokinetic parameter calculations—area under the plasma concentration–time curve (AUC), maximum plasma concentration (C_{max}), i.v. clearance (CL_{iv}), volume of distribution (Vd_{ss}), and half-life ($t_{1/2}$). Other parameters were subsequently calculated on the basis of pharmacokinetic first principles. Oral bioavailability (F) of statins was described by eq. 2:

$$F = F_a \cdot F_g \cdot F_h \tag{2}$$

where F_a represents fraction of drug absorbed; F_g, fraction of drug escaping intestinal extraction; and F_h, fraction of drug escaping hepatic extraction. The F_h was described by eq. 3:

$$F_h = 1 - \frac{CL_{hepatic}}{Q_h} \tag{3}$$

where $CL_{hepatic}$ represents hepatic blood clearance (plasma $CL_{hepatic}$/blood-to-plasma ratio) and Q_h is hepatic blood flow in cynomolgus monkey (44 ml/min/kg) (Hosea et al., 2009). Measured blood-to-plasma ratios of rosuvastatin and pitavastatin in cynomolgus monkey were 0.55 and 0.58, respectively.

The ratio of the AUC (AUCR) of oral statins in the presence (AUC'_{po}) and absence (AUC_{po}) of rifampicin was predicted based on eq. 4.

$$AUCR = \frac{AUC'_{po}}{AUC_{po}} = \frac{F_a'}{F_a} \cdot \frac{F_g'}{F_g} \cdot \frac{F_h'}{F_h} \cdot \frac{(CL_{iv})}{(CL_{iv}')} \tag{4}$$

where $'$ indicates parameters in the presence of rifampicin. For the prediction purposes, it was assumed that rifampicin has no impact on F_a and F_g of both statins, and therefore F_a' and F_g' were the same as in the control phase. F_h' was estimated from the hepatic blood clearance in the presence of rifampicin ($CL_{hepatic}'$), as shown in eq. 5:

$$F_h' = 1 - \frac{CL_{hepatic}'}{Q_h} \tag{5}$$

The CL_{iv} of statins is the sum of hepatic and renal clearance, and, assuming uptake is the rate-determining step for hepatic clearance, it can be expressed as shown in eq. 6:

$$CL_{iv} = CL_{hepatic} + CL_{renal} = CL_{active} + CL_{diff} + CL_{renal} \tag{6}$$

where CL_{renal}, CL_{active}, and CL_{diff} represent renal, sinusoidal active uptake, and passive diffusion clearance, respectively.

In vivo IC_{50} values were estimated using eq. 7 using unbound C_{max} of rifampicin ($[C_{u,max}]$) as independent variable and i.v. clearance of statins as the depending variable.

Downloaded from jpet.aspetjournals.org at ASPET Journals on April 19, 2024

$$CL_{iv}' = \left[\frac{CL_{active}}{1 + \frac{[C_{u,max}]}{IC_{50}}} + CL_{diff}'\right] + CL_{renal}' \quad (7)$$

CL_{diff} was obtained from the data in the presence of the highest rifampicin dose, assuming complete inhibition of active hepatic uptake (eq. 8). It was assumed that rifampicin had no impact on the passive diffusion and renal clearance of both statins, and therefore CL_{diff}' and CL_{renal}' were the same as CL_{diff} and CL_{renal}.

$$CL_{diff} = CL_{iv(+30\ mg/kg\ rifampicin)} - CL_{renal} \quad (8)$$

Geometric mean fold error (gmfe) was calculated to assess the bias of the predicted rosuvastatin and pitavastatin AUCR across rifampicin dose range, as shown in eq. 9 (Gertz et al., 2010):

$$gmfe = 10^{\frac{1}{N}\sum\left|\log\frac{predicted}{observed}\right|} \quad (9)$$

where N represents the number of observations.

Results

In Vitro Uptake Kinetics of Rosuvastatin and Pitavastatin in Monkey Hepatocytes. Uptake of rosuvastatin and pitavastatin (0.1–100 μM) was investigated after incubation with plated cynomolgus monkey hepatocytes, and the kinetic parameters were estimated using the mechanistic two-compartment model. The measured $f_{u,med}$ was 0.83 and 0.99 for rosuvastatin and pitavastatin, respectively, which was used for correction of the initial media concentrations of both drugs. Kinetic profiles of both drugs in monkey hepatocytes demonstrated a saturable and nonsaturable uptake phase (Fig. 1; Table 1). The K_m of rosuvastatin and pitavastatin were 3.29 and 1.99 μM, respectively. Although pitavastatin active uptake clearance was greater than that for rosuvastatin (CL_{active} of 109 μl/min/10^6 cells versus 98.3 μl/min/10^6 cells), the contribution of active process to total uptake was approximately 96% in case of rosuvastatin versus 80% for pitavastatin. The CL_{diff} was approximately 6-fold higher for pitavastatin (26.5 μl/min/10^6 cells) than in the case of rosuvastatin (4.27 μl/min/10^6 cells). Furthermore, the extent of intracellular binding differed between the two probes, as fraction of unbound drug in the cell was 0.25 and 0.024 for rosuvastatin and pitavastatin, respectively.

In Vitro Uptake Inhibition Potency of Rifampicin and Cyclosporine in Monkey Hepatocytes. Both rifampicin and cyclosporine inhibited OATP-mediated rosuvastatin and pitavastatin uptake in a concentration-dependent manner (Fig. 2). For rosuvastatin, up to 88% inhibition was observed after preincubation with rifampicin (Fig. 2A). The uninhibited uptake of rosuvastatin (12%) was in close agreement with the contribution of passive diffusion (4%) estimated from the uptake kinetic study in monkey hepatocytes. The IC_{50} of rifampicin obtained after preincubation with buffer (1.14 μM) was reduced by approximately 2-fold after preincubation with rifampicin (0.54 μM) (Table 2). This marginal (2-fold) effect of preincubation on rifampicin potency seen with rosuvastatin reflects similar findings reported for this inhibitor in human OATP1B1- and OATP1B3-transfected human embryonic kidney 293 (HEK293) cells with estradiol-17β-glucuronide as a probe (2- and 3-fold increase in potency; details in Supplemental Table 4). Cyclosporine showed similar extent of maximal inhibition of rosuvastatin uptake in monkey hepatocytes at the highest concentration (Fig. 2C). However, the increase in cyclosporine inhibition potency following preincubation was more pronounced (7-fold shift) (Table 2).

In the case of pitavastatin, maximal 55% inhibition of uptake was observed at the highest rifampicin concentration and after preincubation with inhibitor (Fig. 2B). There was no significant change in the IC_{50} value after preincubation with rifampicin relative to preincubation with buffer (Table 2). This is in agreement with the data reported in HEK293 cells expressing cynomolgus monkey OATP1B1/1B3 using pitavastatin as a probe, in which preincubation with inhibitor resulted in no significant change in rifampicin IC_{50} (Supplemental Table 4). Discrepancy between the uninhibited uptake (45%) and contribution of passive diffusion (20%) estimated from uptake kinetic data was apparent in the case of pitavastatin. Cyclosporine also showed incomplete inhibition of pitavastatin uptake (Fig. 2D), but, in contrast to rifampicin, its inhibitory potency increased 3.7-fold following

Downloaded from jpet.aspetjournals.org at ASPET Journals on April 19, 2024

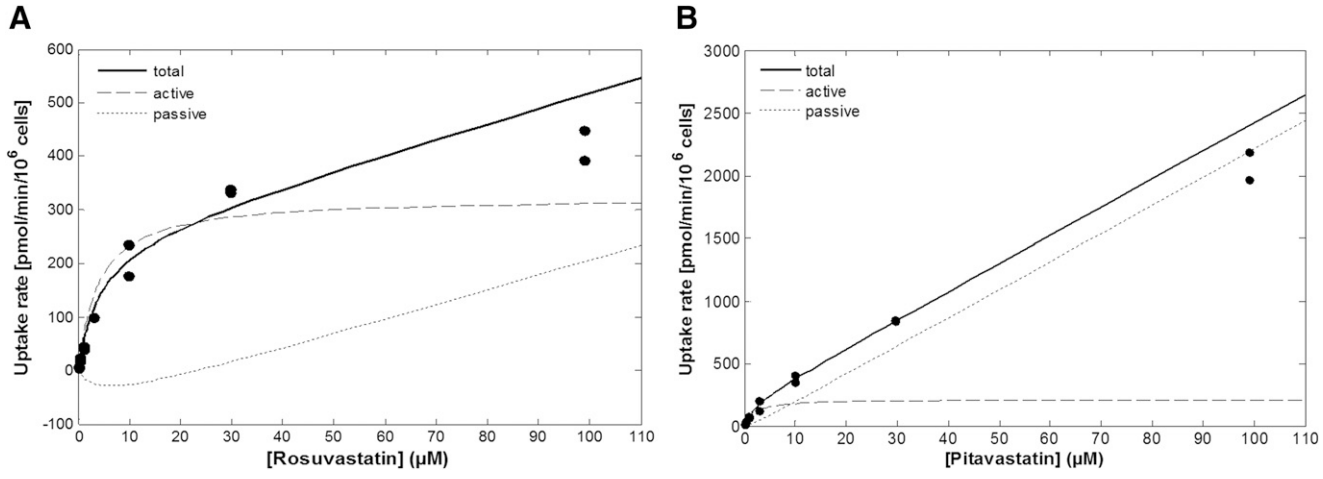

Fig. 1. Uptake kinetic profiles of rosuvastatin (A) and pitavastatin (B) measured in cryopreserved cynomolgus monkey hepatocytes plated for 4 hours. Symbols represent the observed total uptake. Solid, dashed, and dotted lines represent the predicted total, active, and passive diffusion-related uptake, respectively based on a mechanistic two-compartment model.

TABLE 1
Uptake kinetic parameters of rosuvastatin and pitavastatin estimated in plated cynomolgus monkey hepatocytes using a mechanistic two-compartment model

Drug	K_m	V_{max}	$f_{u,cell}$	CL_{diff}	CL_{active}
	μM	pmol/min/10^6 cells		μl/min/10^6 cells	
Rosuvastatin	3.29 ± 0.45	323 ± 44	0.25 ± 0.08	4.27 ± 1.07	98.3
Pitavastatin	1.99 ± 0.31	217 ± 34	0.025 ± 0.009	26.50 ± 2.74	109

preincubation with the inhibitor (Table 2). Additionally, reduction in the steepness of the IC_{50} curves was observed after preincubation in particular with cyclosporine (Fig. 2, C and D). DDI studies with rifamycin SV were also performed to elucidate the possible involvement of NTCP in pitavastatin uptake, which would not be inhibited by rifampicin. The maximum inhibition of pitavastatin uptake increased to 64% after preincubation with rifamycin SV, suggesting some contribution of NTCP in pitavastatin uptake in monkey hepatocytes (Supplemental Fig. 1). No effect of preincubation on rifamycin SV inhibition potency was observed in plated monkey hepatocytes (Table 2). Assuming almost complete inhibition of transporter-mediated uptake of pitavastatin at 1 mM rifamycin SV (Thakare et al., 2017), this uninhibited uptake should represent the contribution of passive diffusion to total cellular uptake, which in this case was higher compared with estimates obtained by mechanistic modeling of kinetic data done over short incubation times. Such incomplete inhibition of uptake for pitavastatin has previously been reported in monkey hepatocytes using rifampicin and cyclosporine (Takahashi et al., 2013) and in human hepatocytes using rifampicin (Pahwa et al., 2017) and may reflect the combination of passive diffusion and involvement of transporter uptake not inhibited by these inhibitors.

Dose-Dependent Effect of Rifampicin on i.v. and Oral Pharmacokinetics of Rosuvastatin and Pitavastatin in Monkeys. Intravenous pharmacokinetics of stable-labeled rosuvastatin and pitavastatin and the oral pharmacokinetics

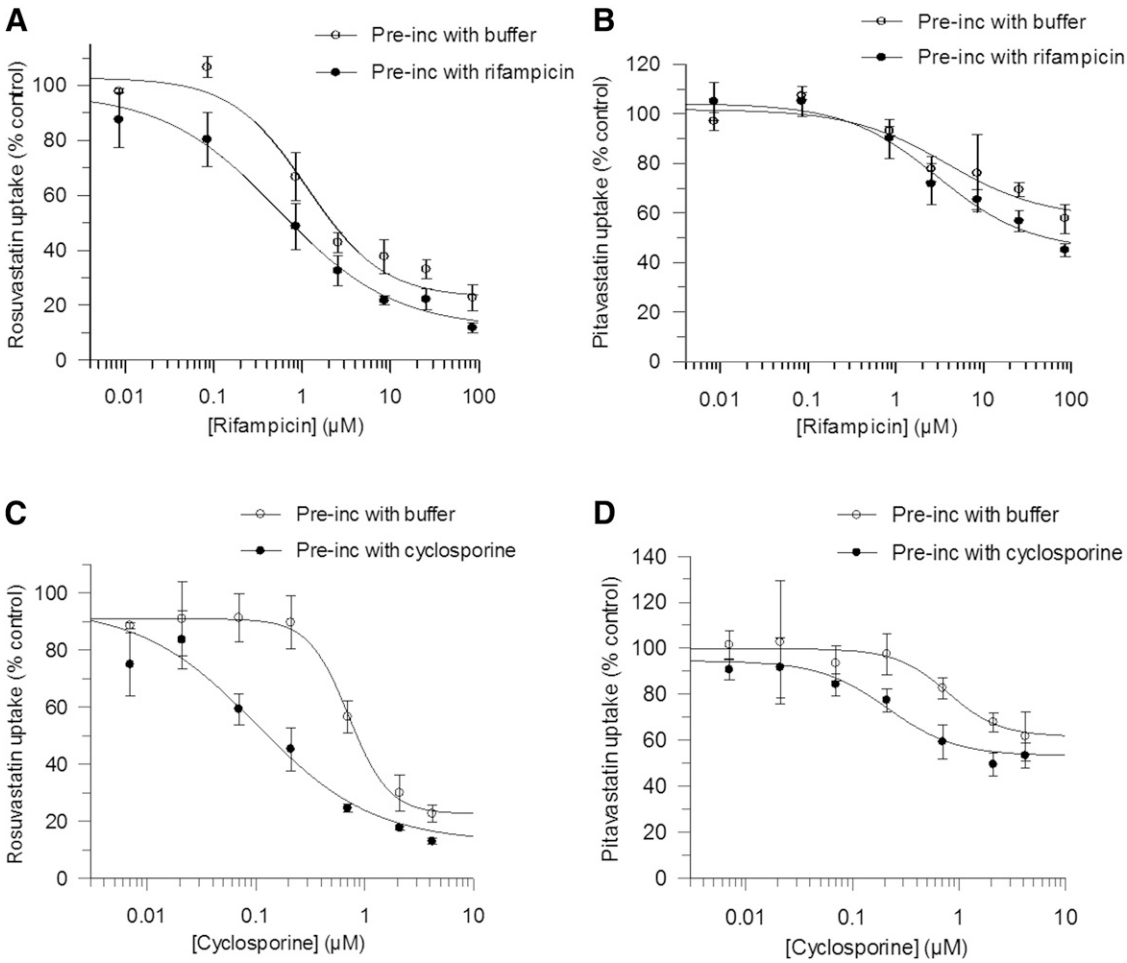

Fig. 2. Rifampicin (A and B) and cyclosporine (C and D) concentration-dependent inhibition of rosuvastatin (A–C) and pitavastatin (B–D) in cryopreserved cynomolgus monkey hepatocytes plated for 4 hours. Preincubation with either buffer or inhibitor (rifampicin 0.01–100 μM, cyclosporine 0.01–6 μM) was performed for 1 hour prior to coincubation with the inhibitor and the probe substrates. Data represent mean uptake ± S.D. of at least triplicate measurements.

Downloaded from jpet.aspetjournals.org at ASPET Journals on April 19, 2024

TABLE 2
In vitro IC_{50} of rifampicin on the OATP-mediated uptake of rosuvastatin and pitavastatin following preincubation with either buffer or inhibitor in cryopreserved plated cynomolgus monkey hepatocytes. The in vivo IC_{50} were estimated based on change in i.v. clearance for these two statins

Substrate	Inhibitor	In vitro IC_{50} (μM)		In vivo IC_{50} (μM)
		Preincubation with Buffer	Preincubation with Inhibitor	
Rosuvastatin	Rifampicin	1.14 ± 0.34**	0.54 ± 0.13**	0.99 ± 3.80
	Cyclosporine	0.72 ± 0.04**	0.10 ± 0.04**	—
Pitavastatin	Rifampicin	3.80 ± 1.82	2.98 ± 0.78	0.22 ± 0.14
	Cyclosporine	0.78 ± 0.14**	0.21 ± 0.06**	—
	Rifamycin SV	6.17 ± 0.96	4.30 ± 1.28	—

Data represent mean ± S.D. of at least triplicate measurements.
**Significant difference between incubation conditions by paired t test ($p \leq 0.01$).

of cold rosuvastatin and pitavastatin were measured in cynomolgus monkeys after single oral ascending does of rifampicin (1, 3, 10, and 30 mg), and compared with the vehicle-only dosing (control). The plasma concentration–time profiles and the corresponding pharmacokinetic parameters are shown in Figs. 3–5 and Table 3. Rosuvastatin i.v. clearance, when dosed along with 30 mg/kg rifampicin, decreased to almost 50% of control, whereas there was no significant change in the volume of distribution. This is in agreement with the previously reported marginal decrease in Vd_{ss} of i.v. rosuvastatin when given with a lower rifampicin dose in cynomolgus monkey (Chu et al., 2015). Oral AUC and C_{max} of rosuvastatin were increased up to 15-fold by the highest dose of rifampicin. In the case of pitavastatin, reduction in i.v. clearance was more prominent (18.0 ml/min/kg versus 4.3 ml/min/kg), and the volume of distribution was reduced from 1.8 (control) to 0.55 l/kg (30 mg/kg rifampicin group). The decrease in i.v. clearance was accompanied by a significant decrease in Vd_{ss}, consistent with a previous report (Takahashi et al., 2013), and, therefore, half-life was not altered significantly by rifampicin. Rifampicin dose-dependent increase in oral pitavastatin plasma exposure was noted with AUC change of up to ~19-fold and C_{max} increase of up to ~12-fold at the highest dose tested (30 mg/kg) compared with the control group.

The lactone forms of orally administered pitavastatin and rosuvastatin were also measured in plasma samples. The plasma AUC of the lactone forms in the absence and presence of rifampicin and the lactone-acid ratios are reported in Supplemental Tables 5 and 6, respectively. No significant increase in the overall lactone plasma AUC was observed for rosuvastatin (Supplemental Table 5). In the case of pitavastatin lactone, a significant increase in its plasma AUC was observed at 3 mg/kg rifampicin. No clear dose-dependent trend in lactone AUC of both statins was apparent. A significant increase in lactone-acid AUC ratios was observed for rosuvastatin only at 1 mg/kg rifampicin relative to control, whereas no significant changes were seen for pitavastatin at any rifampicin dose (Supplemental Table 6). There was an apparent decrease in lactone-acid AUC ratios for both statins, particularly at the highest rifampicin doses. Previously, a decrease and no change in lactone-acid ratio of pitavastatin (in human) and rosuvastatin (in cynomolgus monkey), respectively, were observed in the presence of rifampicin (Prueksaritanont et al., 2014; Chu et al., 2015). Given that the AUCR of a metabolite to parent reflects both the formation and subsequent elimination of the metabolite (Houston, 1981), such behavior is not unexpected.

IVIVE of OATP Inhibition. In vivo inhibitory potency values estimated using unbound C_{max} of rifampicin were 0.99 ± 3.8 and 0.22 ± 0.14 μM against CL_{iv} of rosuvastatin and pitavastatin, respectively (Fig. 6; Table 2). In vitro IC_{50} (0.54 μM), obtained in monkey hepatocytes following rifampicin preincubation and using rosuvastatin as probe substrate, described reasonably well rifampicin dose-dependent inhibition of rosuvastatin CL_{iv}. In contrast, in vitro IC_{50} obtained using pitavastatin as probe substrate did not recover the in vivo inhibition activity of rifampicin against pitavastatin CL_{iv}. However, in vitro IC_{50} generated using rosuvastatin described well the in vivo data of pitavastatin. Subsequently, in vitro IC_{50} value of 0.54 μM and inhibitor unbound C_{max} was employed to predict the rifampicin dose-dependent change in AUC of both statins dosed either i.v. or orally (Fig. 7). The prediction bias calculated from the geometric mean fold error was <1.6-fold for both statins, with 78% and 88% of the predicted AUCR values within 2-fold of the observed data for rosuvastatin and pitavastatin, respectively. An apparent underprediction was noted for the rosuvastatin oral AUCR at higher doses of rifampicin. This is likely due to increased oral absorption as a result of inhibition of rosuvastatin intestinal efflux, which was not captured in the current prediction model (see *Materials and Methods*). To note, exploration of IVIVE using IC_{50} of 0.42 μM obtained in HEK293 cells expressing cOATP1B1 (lowest value compared with those obtained for other OATPs) and using rosuvastatin as an OATP probe (Shen et al., 2013) resulted in either no or marginal improvement in the prediction bias, highlighting the physiologic relevance of monkey hepatocytes for comparison with the inhibition parameters obtained from the in vivo data in a top-down manner.

The F_aF_g of rosuvastatin estimated from the i.v. and oral data of each study arm showed on average a 178% (2.8-fold) increase in rosuvastatin F_aF_g in monkeys receiving 30 mg/kg rifampicin relative to the control arm; this trend was not evident for pitavastatin. Correction of the average predicted AUCR values shown in Fig. 7A by this increase in F_aF_g reduced the underprediction of the magnitude of rosuvastatin DDI at the highest dose of rifampicin (data not shown).

Discussion

In comparison with the increased success of quantitative prediction of CYP-mediated DDIs, the confidence in the successful prediction of OATP-mediated DDIs using in vitro data is still low (Gertz et al., 2013; Prueksaritanont et al., 2014; Jones et al., 2015; Bi et al., 2017; Yoshida et al., 2017).

Downloaded from jpet.aspetjournals.org at ASPET Journals on April 19, 2024

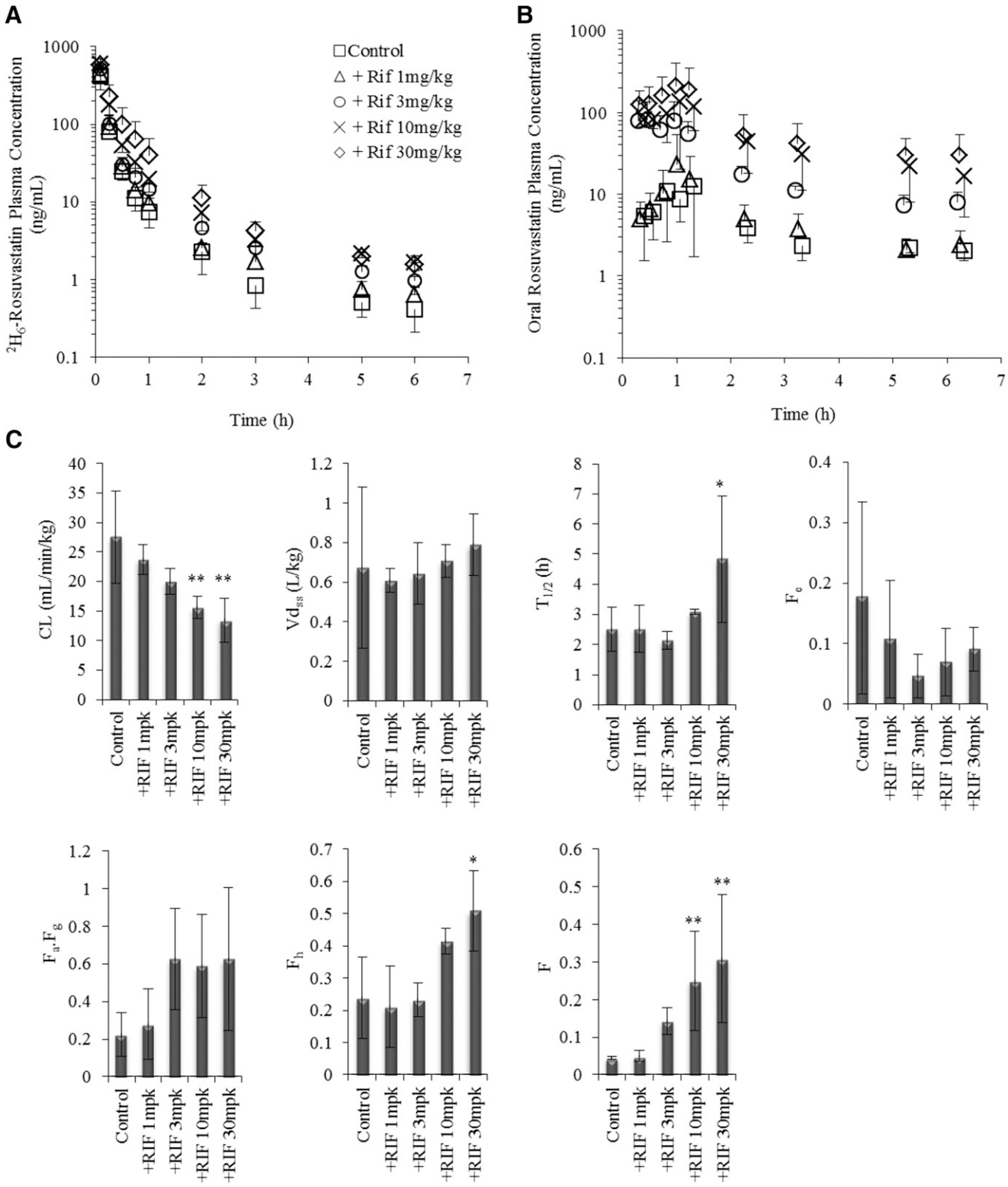

Fig. 3. Effect of single ascending oral doses of rifampicin on the i.v. and oral pharmacokinetics of rosuvastatin in cynomolgus monkey. Plasma concentration–time profiles of i.v. $^2H_6$-rosuvastatin (A) and oral cold rosuvastatin (B) and the estimated pharmacokinetics (C) are depicted. Pharmacokinetic parameters were estimated, with each monkey serving as its own control. Data represent mean ± S.D. (n = 4). One-way analysis of variance with Dunnett's multiple comparisons test was employed to test significance with $^*p < 0.05$; $^{**}p < 0.01$.

Therefore, the objective of our study was to evaluate the IVIVE of OATP inhibition potential using cynomolgus monkey as a preclinical model and to gain confidence in mechanistic translational approach to predict clinical DDIs mediated by these transporters. Furthermore, it was aimed at improving our understanding of the utility of the cynomolgus monkey as a model for humans to drive evaluation of clearance mechanisms (rate-determining step) and DDI risk. Collective results

Downloaded from jpet.aspetjournals.org at ASPET Journals on April 19, 2024

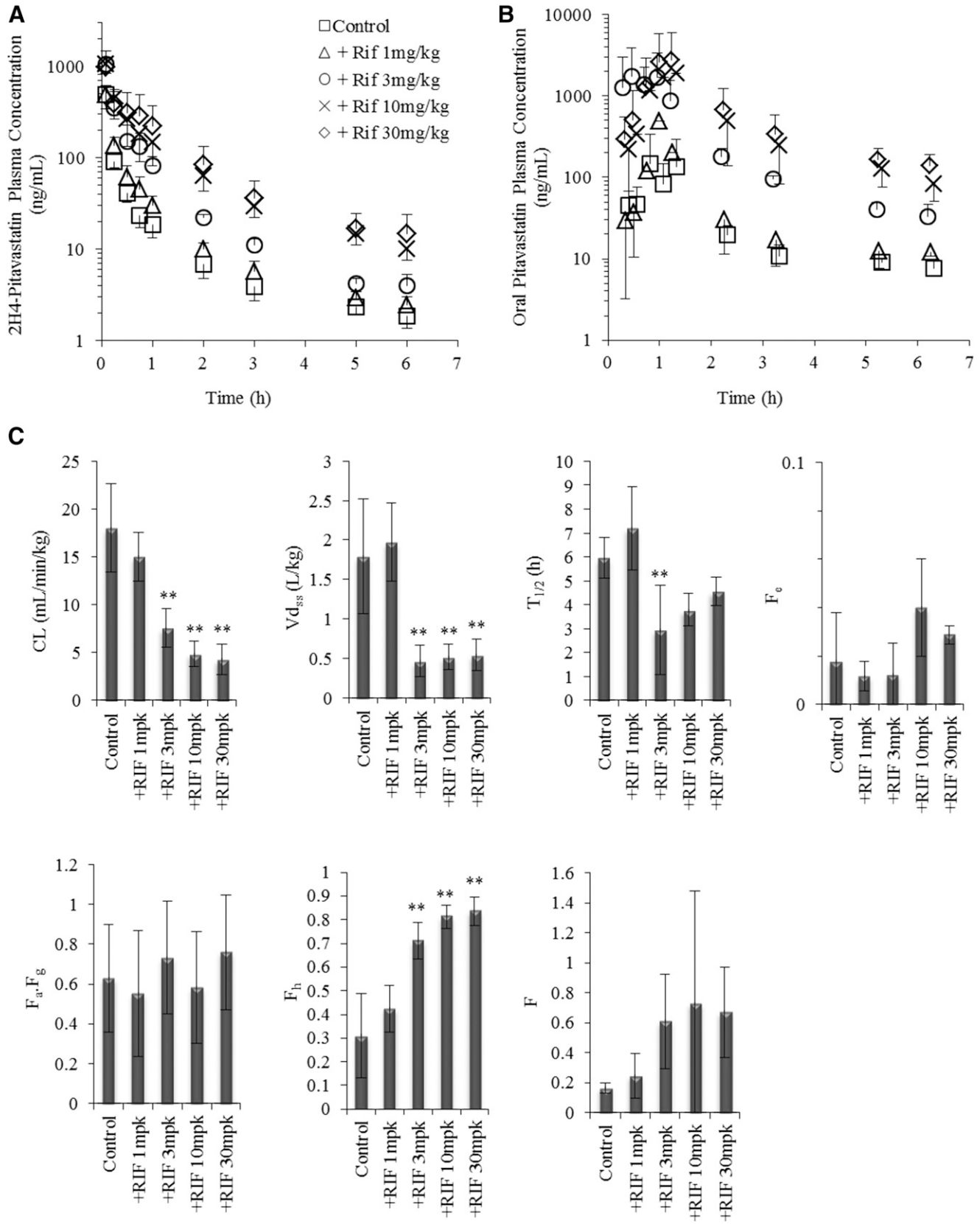

Fig. 4. Effect of single ascending oral doses of rifampicin on the i.v. and oral pharmacokinetics of pitavastatin in cynomolgus monkey. Plasma concentration–time profiles of i.v. $^{2}H_{4}$-pitavastatin (A) and oral cold pitavastatin (B) and the estimated pharmacokinetics (C) are depicted. Pharmacokinetics parameters were estimated, with each monkey serving as its own control. Data represent mean ± S.D. (n = 4). One-way analysis of variance with Dunnett's multiple comparisons test was employed to test significance with $^{*}p < 0.05$; $^{**}p < 0.01$.

Downloaded from jpet.aspetjournals.org at ASPET Journals on April 19, 2024

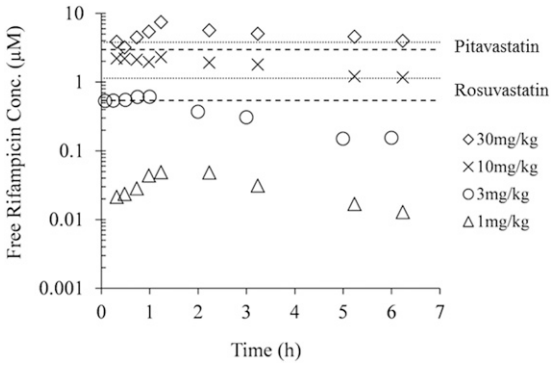

Fig. 5. Rifampicin mean unbound plasma concentration–time profiles at different doses following oral administration in cynomolgus monkey. Horizontal lines represent in vitro IC_{50} values estimated using rosuvastatin and pitavastatin as probe substrates following preincubation with buffer (dotted) or rifampicin (dashed) (Table 2).

suggest that quantitative OATP1B DDI predictions can be made from in vitro IC_{50} measured in primary hepatocytes using multiple probe substrates following preincubation with the inhibitor.

In the current study, both rosuvastatin and pitavastatin showed a high affinity for uptake transport in monkey hepatocytes (Table 1). Rosuvastatin CL_{active} was approximately 4-fold greater in the current monkey donor investigated compared with the previous data (Shen et al., 2013), possibly reflecting donor differences in the transporter activity, as the estimated K_m values were comparable. Although CL_{diff} was about 6-fold greater in the donor used in the current study, contribution of the passive process to the overall uptake of rosuvastatin (4.2%) was in agreement with previous reports in monkey hepatocytes (Shen et al., 2013).

In this study, the effect of preincubation on the inhibition of OATP-mediated rosuvastatin and pitavastatin uptake in monkey hepatocytes was investigated using prototypical inhibitors rifampicin and cyclosporine. In contrast to the marginal decrease in rifampicin IC_{50} after preincubation, more pronounced increase in cyclosporine potency (up to 7-fold) was seen regardless of the substrate probe used. This clear preincubation effect on cyclosporine inhibition potency demonstrated in this work in monkey hepatocytes is in agreement with previous literature reports on this inhibitor. But the reported magnitude of shift in cyclosporine potency varied between in vitro systems and probes used (Supplemental Table 4), with up to 22- and 23-fold increase in cyclosporine potency noted after preincubation in human and monkey OATP1B1-transfected HEK293 cells, respectively, highlighting that the effect of preincubation on the potency of OATP inhibitors is dependent not only on the substrate used but also on the cellular system investigated.

Incomplete inhibition of uptake was observed for pitavastatin in the current study. As a number of reports demonstrated the contribution of sodium-dependent NTCP to the uptake of pitavastatin and rosuvastatin in human (Bi et al., 2013, 2017) and monkey hepatocytes (Thakare et al., 2017), pitavastatin uptake was further evaluated in the presence of rifamycin SV. Although rifamycin SV increased the maximal inhibition of pitavastatin uptake in monkey hepatocytes, incomplete inhibition of uptake was still evident, highlighting potentially lower transporter activity and/or higher passive contribution in the pooled donor investigated.

TABLE 3
Summary of pharmacokinetic estimates of pitavastatin and rosuvastatin in the presence of single ascending doses of rifampicin in cynomolgus monkey

	Control	+Rifampicin 1 mg/kg	+Rifampicin 3 mg/kg	+Rifampicin 10 mg/kg	+Rifampicin 30 mg/kg
	Mean ± S.D.	Mean ± S.D.	Mean ± S.D.	Mean ± S.D.	Mean ± S.D.
Pitavastatin					
CL (ml/min/kg)	18.0 ± 4.6	15.0 ± 2.5	7.5 ± 2.0	4.9 ± 1.3	4.3 ± 1.6
Fold change		0.83	0.42**	0.27**	0.24**
Vd_{ss} (l/kg)	1.79 ± 0.72	1.97 ± 0.50	0.47 ± 0.20	0.52 ± 0.16	0.55 ± 0.20
Fold change		1.10	0.26**	0.29**	0.30**
$t_{1/2}$ (h)	5.9 ± 0.9	7.2 ± 1.7	2.9 ± 1.9	3.8 ± 0.7	4.5 ± 0.6
Fold change		1.21	0.50**	0.63	0.76
Oral AUC_{last} (ng.h/ml)	299 ± 146	515 ± 417	2690 ± 2710	4070 ± 4357	5808 ± 4579
Fold change		1.72	8.99**	13.60**	19.41**
Oral C_{max} (ng/ml)	225 ± 200	520 ± 822	2730 ± 2040	1920 ± 2950	2780 ± 3166
Fold change		2.31	12.13**	8.53**	12.36**
Rosuvastatin					
CL (ml/min/kg)	27.5 ± 7.8	23.6 ± 2.4	20.0 ± 2.1	15.6 ± 1.9	13.4 ± 3.7
Fold change		0.86	0.73	0.57**	0.49**
Vd_{ss} (l/kg)	0.67 ± 0.41	0.61 ± 0.06	0.64 ± 0.16	0.71 ± 0.08	0.79 ± 0.16
Fold change		0.91	0.96	1.05	1.17
$t_{1/2}$ (h)	2.5 ± 0.7	2.5 ± 0.8	2.1 ± 0.3	3.1 ± 0.1	4.8 ± 2.0
Fold change		1.01	0.86	1.23	1.93*
Oral AUC_{last} (ng.h/ml)	49 ± 12	63 ± 28	232 ± 43	467 ± 267	744 ± 512
Fold change		1.28	4.68**	9.41**	15.01**
Oral C_{max} (ng/ml)	15 ± 11	24 ± 29	122 ± 46	150 ± 100	227 ± 169
Fold change		1.54	7.72**	9.49**	14.37**
Rifampicin					
Oral AUC_{last} (ng.h/ml)		985 ± 396	11,300 ± 3260	70,100 ± 10,800	240,000 ± 73,900
Dose-normalized change related to 1 mg/kg		—	3.8	7.1	8.1
Oral C_{max} (ng/ml)		176 ± 99	2050 ± 245	7980 ± 2480	24,200 ± 14,100
Dose-normalized change related to 1 mg/kg		—	3.8	4.5	4.6

Data represent mean ± S.D. (N = 4). One-way analysis of variance with Dunnett's multiple comparisons test was employed to test significance with *$p < 0.05$; **$p < 0.01$.

Downloaded from jpet.aspetjournals.org at ASPET Journals on April 19, 2024

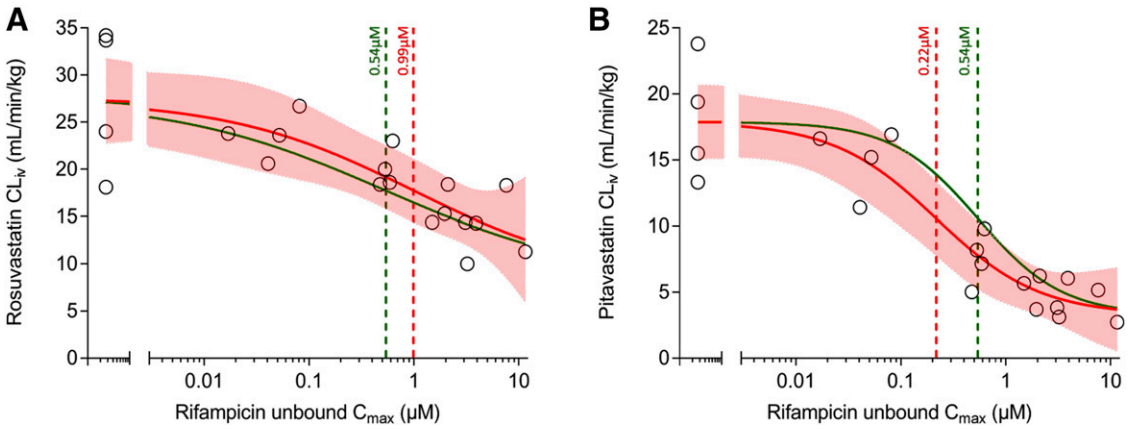

Fig. 6. IVIVE of hepatic uptake inhibition by rifampicin in cynomolgus monkey. Plots depict rifampicin plasma concentration-dependent inhibition of i.v. clearance of rosuvastatin (A) and pitavastatin (B). Data were fitted to eq. 7 to estimate in vivo IC_{50} with each statin (red curves with shaded area: 95% confidence interval). Additionally, change in i.v. clearance was predicted using in vitro IC_{50} obtained in monkey hepatocytes following preincubation with rifampicin with rosuvastatin as a probe (green curve). Vertical lines represent in vivo and in vitro IC_{50} values (Table 2).

The quantitative translation of interaction noted in monkeys to humans may not be straightforward due to possible species difference in the multiple mechanisms involved in the clearance. However, several recent reports suggested good agreement between cynomolgus monkeys and humans in the magnitude of DDIs with rifampicin as an OATP inhibitor (Shen et al., 2013; Watanabe et al., 2015). In this study, rifampicin showed a dose-dependent effect with no further change in statins pharmacokinetics between rifampicin doses of 10 and 30 mg/kg in monkeys. The unbound C_{max} of rifampicin achieved (~2–7 μM) at these doses is comparable to the unbound C_{max} in humans following single 600 mg dose (Varma et al., 2012; Prueksaritanont et al., 2014; Yoshikado et al., 2017). However, the magnitude of change in the oral AUC for both statins observed in the cynomolgus monkeys (~15 to 20-fold, Table 3) is much higher than noted in humans (AUCR ~5) (Prueksaritanont et al., 2014). In contrast, an earlier study showed ~3-fold increase in oral rosuvastatin AUC in cynomolgus monkey with rifampicin dose of 15 mg/kg orally (Shen et al., 2013). Although the reasons for such a difference are not apparent, a relatively smaller magnitude of rosuvastatin DDI in humans may be attributed to the contribution of OATP2B1 to its hepatic uptake, which is not affected by rifampicin at in vivo relevant plasma concentrations (OATP2B1 in vitro $IC_{50} > 60$ μM). However, the contribution of OATP2B1 to rosuvastatin hepatic uptake in monkey is likely to be minor because of its relatively low expression in cynomolgus liver (Wang et al., 2015). In addition to OATPs, both rosuvastatin and pitavastatin are substrates of efflux transporters, such as multidrug resistance protein

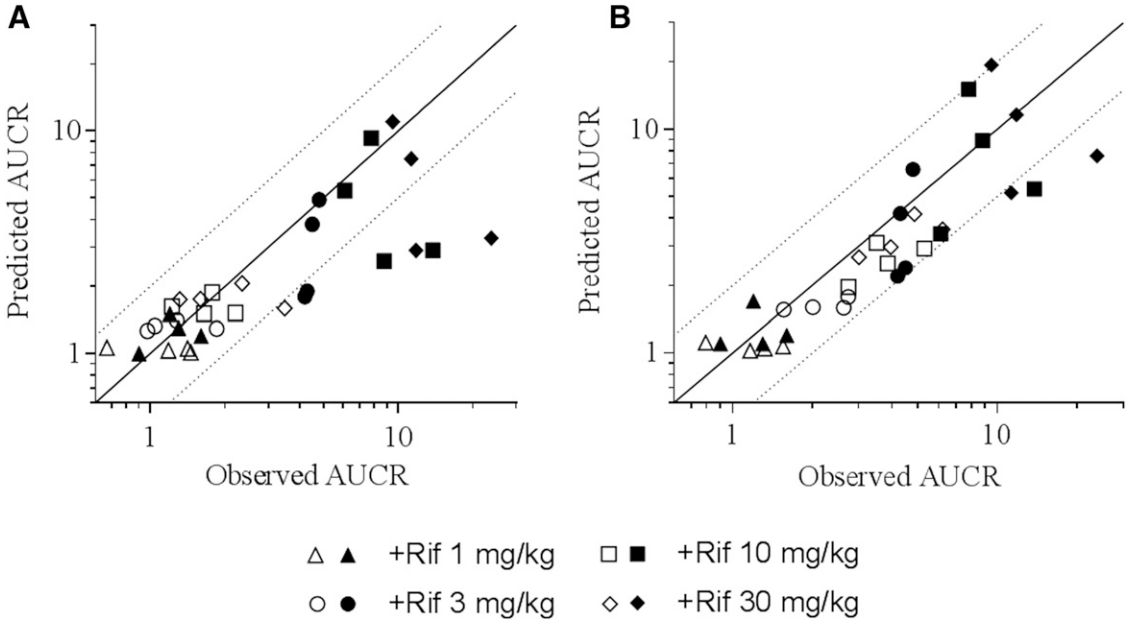

Fig. 7. Predicted versus observed interactions between rifampicin and rosuvastatin (A) or pitavastatin (B), when administered with single ascending oral doses of rifampicin. Change in exposure (AUCR) of i.v. (open symbols) and oral (closed symbols) statins was predicted based on eqs. 4–7 using the measured unbound C_{max} of rifampicin and in vitro IC_{50} of 0.54 μM. Each monkey served as its own control in calculating the AUCR. Solid and dotted lines represent the line of unity and 2-fold error, respectively.

Downloaded from jpet.aspetjournals.org at ASPET Journals on April 19, 2024

2 (MRP2) and breast cancer resistance protein (BCRP) (Prueksaritanont et al., 2014; Lee et al., 2015). As rifampicin is also indicated as a substrate of OATP1Bs (Yamaguchi et al., 2011), its inhibitory effect on the biliary efflux of rosuvastatin and pitavastatin was considered. Previously, Chu et al. (2015) showed relatively weak inhibition of cynomolgus MRP2 (cMRP2) by rifampicin in HEK293 cells (IC_{50} of 118 μM). Assuming the reported unbound liver-to-plasma concentration ratio (Kp_{uu}) of 3.3 for rifampicin in humans (Chu et al., 2015) is comparable to that in cynomolgus monkeys, the IC_{50} for cMRP2 is much higher than the estimated rifampicin-unbound liver concentrations (approximately 23 μM at the highest rifampicin dose used), suggesting that the increase in plasma exposure of both statins is unlikely to be caused by MRP2 inhibition. In case of potential MRP2 inhibition, expectation is that liver AUC will change, consistent with an understanding of the rate-determining processes that affect hepatic exposure of these drugs (Tsamandouras et al., 2015).

The increase in F_aF_g of rosuvastatin seen in this study is most likely attributed to the effect of rifampicin on intestinal BCRP. Rosuvastatin absorption in humans is approximately 50% of the oral dose (Martin et al., 2003), whereas only ~20% was noted in monkeys (control arm). This difference in F_aF_g values suggests species differences in the expression of the intestinal transporters, including BCRP. This is supported by previous reports of generally greater mRNA expression of intestinal efflux transporters in cynomolgus monkeys relative to humans (60-fold difference in the case of BCRP) (Takahashi et al., 2008). Although we cannot assess the differential effects of intestinal OATP2B1 uptake versus BCRP efflux definitively, increased absorption following rifampicin administration implies that BCRP efflux plays a prominent role in the oral absorption of rosuvastatin in monkeys. In contrast, pitavastatin is a highly permeable drug, and the F_aF_g (~0.7 in control arm) is not expected to be limited by intestinal efflux (El-Kattan et al., 2016). Taken together, the current monkey study suggests potential contribution of intestinal efflux inhibition to the rifampicin-rosuvastatin DDIs.

The rich dataset of rifampicin dose-dependent effect on two statins simultaneously dosed i.v. and orally was leveraged to investigate the IVIVE of OATP1B-mediated DDIs. The in vivo IC_{50} values, estimated using i.v. clearance of rosuvastatin/pitavastatin and unbound C_{max} of rifampicin, were within 2.5-fold of the in vitro IC_{50} (0.54 μM) obtained following preincubation with rifampicin and using rosuvastatin as probe substrate in primary monkey hepatocytes. This in vitro IC_{50} predicted the AUCR of both statins after i.v. and oral dosing with high accuracy (minimum 78% within 2-fold of the observed data), when employing the static mechanistic model (eq. 7). In contrast, the in vitro IC_{50} obtained under all other experimental conditions (Table 2) considerably underpredicted the fold change in the AUC of statins investigated. Consistent with the IVIVE noted in this work in monkeys, Varma et al. (2014) demonstrated that similar inhibition potency (0.5 μM), obtained using OATP1B1-transfected cells, correctly predicted rifampicin clinical DDIs when using a static mechanistic model (>85% within 2-fold of observed AUCRs, $n = 22$). Overall, the current monkey study validates mechanistic translational framework to predict OATP1B-mediated DDIs in humans.

Substrate-dependent inhibition was argued as a potential cause for concern in prospective prediction of OATP1B-mediated interactions (Noé et al., 2007; Izumi et al., 2013; Zamek-Gliszczynski et al., 2013). We report almost 6-fold difference in rifampicin unbound IC_{50} measured with preincubation when using rosuvastatin (0.54 μM) versus pitavastatin (3.0 μM) (Table 2). Interestingly, the change in i.v. clearance and oral exposure of both rosuvastatin and pitavastatin is recovered well only by the rifampicin in vitro IC_{50} measured against rosuvastatin (Figs. 6 and 7). Based on these findings, it can be inferred that: 1) substrate-dependent inhibitory potency noted in vitro may not translate to differences in vivo, 2) IC_{50} measured following preincubation with inhibitor is needed for quantitative prediction of OATP-mediated DDIs, and 3) in vitro inhibition studies should consider more than one probe substrate, and the most potent measurement should be employed for reliable prospective predictions. Of note, plasma coproporphyrins (I and III) have recently been described as selective and sensitive OATP1B biomarkers in both cynomolgus monkeys and humans (Shen et al., 2016; Barnett et al., 2017). Therefore, the coordinated use of the cynomolgus monkey (prehuman dosing), with measurements of changes in biomarker exposure in Phase 1, could be leveraged to quickly discharge OATP1B DDI risk. Given that current regulatory agency–driven OATP1B DDI risk analyses are conservative and present a relatively high false-positive rate (~30%) (Vaidyanathan et al., 2016), consideration of such approaches is warranted.

In summary, our studies using the cynomolgus monkey as a preclinical model demonstrated a rational translation of in vitro inhibition potency in predicting OATP1B DDIs. Rifampicin in vitro inhibition potency measured using monkey hepatocytes was influenced by a preincubation step and/or the probe substrate employed. However, in vivo IC_{50} values obtained from the change in rosuvastatin or pitavastatin i.v. clearance as a function of rifampicin unbound C_{max} were not statistically different. Additionally, the most potent IC_{50} obtained under preincubation conditions provided good quantitative predictions of fold changes in plasma AUC for both statins following oral administration. Collectively, these findings suggest the need for employing multiple probe substrates and a preincubation step when conducting in vitro inhibition studies. Finally, this study emphasizes further the utility of cynomolgus monkey as a preclinical model in supporting the early assessment of OATP-mediated DDI risk.

Acknowledgments

We thank Dr. R. Scott Obach, Dr. Emi Kimoto, Dr. Elaine Tseng, and Dr. Theunis Goosen (Pfizer) for valuable inputs during this work. Sangwoo Ryu and Keith Riccardi (Pfizer) are acknowledged for conducting plasma protein–binding measurements. Susan Murby and Dr. David Hallifax (University of Manchester) are acknowledged for assistance with the analytical assays.

Authorship Contributions

Participated in research design: Ufuk, Kosa, Gao, Bi, Rodrigues, Tremaine, Varma, Houston, Galetin.

Conducted experiments: Ufuk, Kosa, Gao, Bi, Modi, Gates.

Contributed new reagents or analytic tools: Gao.

Performed data analysis: Ufuk, Kosa, Varma, Houston, Galetin.

Wrote or contributed to the writing of the manuscript: Ufuk, Kosa, Gao, Modi, Gates, Rodrigues, Tremaine, Varma, Houston, Galetin.

References

Amundsen R, Christensen H, Zabihyan B, and Asberg A (2010) Cyclosporine A, but not tacrolimus, shows relevant inhibition of organic anion-transporting protein 1B1-mediated transport of atorvastatin. *Drug Metab Dispos* **38**:1499–1504.

Barnett S, Ogungbenro K, Menochet K, Shen H, Lai Y, Humphreys WG, and Galetin A (2017) Gaining mechanistic insight into coproporphyrin I as endogenous

Downloaded from jpet.aspetjournals.org at ASPET Journals on April 19, 2024

biomarker for OATP1B-mediated drug-drug interactions using population pharmacokinetic modelling and simulation. *Clin Pharmacol Ther* DOI: 10.1002/cpt.983 [published ahead of print].
Bi YA, Qiu X, Rotter CJ, Kimoto E, Piotrowski M, Varma MV, Ei-Kattan AF, and Lai Y (2013) Quantitative assessment of the contribution of sodium-dependent taurocholate co-transporting polypeptide (NTCP) to the hepatic uptake of rosuvastatin, pitavastatin and fluvastatin. *Biopharm Drug Dispos* **34**:452–461.
Bi YA, Scialis RJ, Lazzaro S, Mathialagan S, Kimoto E, Keefer J, Zhang H, Vildhede AM, Costales C, Rodrigues AD, et al. (2017) Reliable rate measurements for active and passive hepatic uptake using plated human hepatocytes. *AAPS J* **19**:787–796.
Chu X, Shih SJ, Shaw R, Hentze H, Chan GH, Owens K, Wang S, Cai X, Newton D, Castro-Perez J, et al. (2015) Evaluation of cynomolgus monkeys for the identification of endogenous biomarkers for hepatic transporter inhibition and as a translatable model to predict pharmacokinetic interactions with statins in humans. *Drug Metab Dispos* **43**:851–863.
Ebeling M, Kung E, See A, Broger C, Steiner G, Berrera M, Heckel T, Iniguez L, Albert T, Schmucki R, et al. (2011) Genome-based analysis of the nonhuman primate Macaca fascicularis as a model for drug safety assessment. *Genome Res* **21**: 1746–1756.
El-Kattan AF, Varma MV, Steyn SJ, Scott DO, Maurer TS, and Bergman A (2016) Projecting ADME behavior and drug-drug interactions in early discovery and development: application of the extended clearance classification system. *Pharm Res* **33**:3021–3030.
Galetin A, Zhao P, and Huang SM (2017) Physiologically based pharmacokinetic modeling of drug transporters to facilitate individualized dose prediction. *J Pharm Sci* **106**:2204–2208.
Gertz M, Cartwright CM, Hobbs MJ, Kenworthy KE, Rowland M, Houston JB, and Galetin A (2013) Cyclosporine inhibition of hepatic and intestinal CYP3A4, uptake and efflux transporters: application of PBPK modeling in the assessment of drug-drug interaction potential. *Pharm Res* **30**:761–780.
Gertz M, Harrison A, Houston JB, and Galetin A (2010) Prediction of human intestinal first-pass metabolism of 25 CYP3A substrates from in vitro clearance and permeability data. *Drug Metab Dispos* **38**:1147–1158.
Giacomini KM, Huang SM, Tweedie DJ, Benet LZ, Brouwer KL, Chu X, Dahlin A, Evers R, Fischer V, Hillgren KM, et al. (2010) Membrane transporters in drug development. *Nat Rev Drug Discov* **9**:215–236.
Hosea NA, Collard WT, Cole S, Maurer TS, Fang RX, Jones H, Kakar SM, Nakai Y, Smith BJ, Webster R, et al. (2009) Prediction of human pharmacokinetics from preclinical information: comparative accuracy of quantitative prediction approaches. *J Clin Pharmacol* **49**:513–533.
Houston JB (1981) Drug metabolite kinetics. *Pharmacol Ther* **15**:521–552.
Izumi S, Nozaki Y, Komori T, Maeda K, Takenaka O, Kusano K, Yoshimura T, Kusuhara H, and Sugiyama Y (2013) Substrate-dependent inhibition of organic anion transporting polypeptide 1B1: comparative analysis with prototypical probe substrates estradiol-17beta-glucuronide, estrone-3-sulfate, and sulfobromophthalein. *Drug Metab Dispos* **41**:1859–1866.
Izumi S, Nozaki Y, Maeda K, Komori T, Takenaka O, Kusuhara H, and Sugiyama Y (2015) Investigation of the impact of substrate selection on in vitro organic anion transporting polypeptide 1B1 inhibition profiles for the prediction of drug-drug interactions. *Drug Metab Dispos* **43**:235–247.
Jones HM, Chen Y, Gibson C, Heimbach T, Parrott N, Peters SA, Snoeys J, Upreti VV, Zheng M, and Hall SD (2015) Physiologically based pharmacokinetic modeling in drug discovery and development: a pharmaceutical industry perspective. *Clin Pharmacol Ther* **97**:247–262.
Lee CA, O'Connor MA, Ritchie TK, Galetin A, Cook JA, Ragueneau-Majlessi I, Ellens H, Feng B, Taub ME, Paine MF, et al. (2015) Breast cancer resistance protein (ABCG2) in clinical pharmacokinetics and drug interactions: practical recommendations for clinical victim and perpetrator drug-drug interaction study design. *Drug Metab Dispos* **43**:490–509.
Li R, Barton HA, and Varma MV (2014) Prediction of pharmacokinetics and drug-drug interactions when hepatic transporters are involved. *Clin Pharmacokinet* **53**: 659–678.
Martin PD, Warwick MJ, Dane AL, Brindley C, and Short T (2003) Absolute oral bioavailability of rosuvastatin in healthy white adult male volunteers. *Clin Ther* **25**:2553–2563.
Ménochet K, Kenworthy KE, Houston JB, and Galetin A (2012) Simultaneous assessment of uptake and metabolism in rat hepatocytes: a comprehensive mechanistic model. *J Pharmacol Exp Ther* **341**:2–15.
Noé J, Portmann R, Brun ME, and Funk C (2007) Substrate-dependent drug-drug interactions between gemfibrozil, fluvastatin and other organic anion-transporting peptide (OATP) substrates on OATP1B1, OATP2B1, and OATP1B3. *Drug Metab Dispos* **35**:1308–1314.
Pahwa S, Alam K, Crowe A, Farasyn T, Neuhoff S, Hatley O, Ding K, and Yue W (2017) Pretreatment with rifampicin and tyrosine kinase inhibitor dasatinib potentiates the inhibitory effects toward OATP1B1- and OATP1B3-mediated transport. *J Pharm Sci* **106**:2123–2135.
Prueksaritanont T, Chu X, Evers R, Klopfer SO, Caro L, Kothare PA, Dempsey C, Rasmussen S, Houle R, Chan G, et al. (2014) Pitavastatin is a more sensitive and selective organic anion-transporting polypeptide 1B clinical probe than rosuvastatin. *Br J Clin Pharmacol* **78**:587–598.
Reinoso RF, Telfer BA, Brennan BS, and Rowland M (2001) Uptake of teicoplanin by isolated rat hepatocytes: comparison with in vivo hepatic distribution. *Drug Metab Dispos* **29**:453–459.
Shen H, Dai J, Liu T, Cheng Y, Chen W, Freeden C, Zhang Y, Humphreys WG, Marathe P, and Lai Y (2016) Coproporphyrins I and III as functional markers of OATP1B activity: in vitro and in vivo evaluation in preclinical species. *J Pharmacol Exp Ther* **357**:382–393.
Shen H, Su H, Liu T, Yao M, Mintier G, Li L, Fancher RM, Iyer R, Marathe P, Lai Y, et al. (2015) Evaluation of rosuvastatin as an organic anion transporting polypeptide (OATP) probe substrate: in vitro transport and in vivo disposition in cynomolgus monkeys. *J Pharmacol Exp Ther* **353**:380–391.
Shen H, Yang Z, Mintier G, Han YH, Chen C, Balimane P, Jemal M, Zhao W, Zhang R, Kallipatti S, et al. (2013) Cynomolgus monkey as a potential model to assess drug interactions involving hepatic organic anion transporting polypeptides: in vitro, in vivo, and in vitro-to-in vivo extrapolation. *J Pharmacol Exp Ther* **344**:673–685.
Takahashi M, Washio T, Suzuki N, Igeta K, Fujii Y, Hayashi M, Shirasaka Y, and Yamashita S (2008) Characterization of gastrointestinal drug absorption in cynomolgus monkeys. *Mol Pharm* **5**:340–348.
Takahashi T, Ohtsuka T, Uno Y, Utoh M, Yamazaki H, and Kume T (2016) Preincubation with cyclosporine A potentiates its inhibitory effects on pitavastatin uptake mediated by recombinantly expressed cynomolgus monkey hepatic organic anion transporting polypeptide. *Biopharm Drug Dispos* **37**:479–490.
Takahashi T, Ohtsuka T, Yoshikawa T, Tatekawa I, Uno Y, Utoh M, Yamazaki H, and Kume T (2013) Pitavastatin as an in vivo probe for studying hepatic organic anion transporting polypeptide-mediated drug-drug interactions in cynomolgus monkeys. *Drug Metab Dispos* **41**:1875–1882.
Thakare R, Gao H, Kosa RE, Bi YA, Varma MVS, Cerny MA, Sharma R, Kuhn M, Huang B, Liu Y, et al. (2017) Leveraging of rifampicin-dosed cynomolgus monkeys to identify bile acid 3-O-sulfate conjugates as potential novel biomarkers for organic anion-transporting polypeptides. *Drug Metab Dispos* **45**:721–733.
Tsamandouras N, Dickinson G, Guo Y, Hall S, Rostami-Hodjegan A, Galetin A, and Aarons L (2015) Development and application of a mechanistic pharmacokinetic model for simvastatin and its active metabolite simvastatin acid using an integrated population PBPK approach. *Pharm Res* **32**:1864–1883.
Vaidyanathan J, Yoshida K, Arya V, and Zhang L (2016) Comparing various in vitro prediction criteria to assess the potential of a new molecular entity to inhibit organic anion transporting polypeptide 1B1. *J Clin Pharmacol* **56** (Suppl 7): S59–S72.
Varma MV, Bi YA, Kimoto E, and Lin J (2014) Quantitative prediction of transporter- and enzyme-mediated clinical drug-drug interactions of organic anion-transporting polypeptide 1B1 substrates using a mechanistic net-effect model. *J Pharmacol Exp Ther* **351**:214–223.
Varma MV, El-Kattan AF, Feng B, Steyn SJ, Maurer TS, Scott DO, Rodrigues AD, and Tremaine LM (2017) Extended Clearance Classification System (ECCS) informed approach for evaluating investigational drugs as substrates of drug transporters. *Clin Pharmacol Ther* **102**:33–36.
Varma MV, Lai Y, Feng B, Litchfield J, Goosen TC, and Bergman A (2012) Physiologically based modeling of pravastatin transporter-mediated hepatobiliary disposition and drug-drug interactions. *Pharm Res* **29**:2860–2873.
Varma MV, Steyn SJ, Allerton C, and El-Kattan AF (2015) Predicting clearance mechanism in drug discovery: Extended Clearance Classification System (ECCS). *Pharm Res* **32**:3785–3802.
Wang L, Prasad B, Salphati L, Chu X, Gupta A, Hop CE, Evers R, and Unadkat JD (2015) Interspecies variability in expression of hepatobiliary transporters across human, dog, monkey, and rat as determined by quantitative proteomics. *Drug Metab Dispos* **43**:367–374.
Watanabe M, Watanabe T, Yabuki M, and Tamai I (2015) Dehydroepiandrosterone sulfate, a useful endogenous probe for evaluation of drug-drug interaction on hepatic organic anion transporting polypeptide (OATP) in cynomolgus monkeys. *Drug Metab Pharmacokinet* **30**:198–204.
Yamaguchi H, Takeuchi T, Okada M, Kobayashi M, Unno M, Abe T, Goto J, Hishinuma T, Shimada M, and Mano N (2011) Screening of antibiotics that interact with organic anion-transporting polypeptides 1B1 and 1B3 using fluorescent probes. *Biol Pharm Bull* **34**:389–395.
Yoshida K, Maeda K, and Sugiyama Y (2012) Transporter-mediated drug–drug interactions involving OATP substrates: predictions based on in vitro inhibition studies. *Clin Pharmacol Ther* **91**:1053–1064.
Yoshida K, Zhao P, Zhang L, Abernethy DR, Rekic D, Reynolds KS, Galetin A, and Huang SM (2017) In vitro-in vivo extrapolation of metabolism- and transporter-mediated drug-drug interactions: overview of basic prediction methods. *J Pharm Sci* **106**:2209–2213.
Yoshikado T, Maeda K, Furihata S, Terashima H, Nakayama T, Ishigame K, Tsunemoto K, Kusuhara H, Furihata KI, and Sugiyama Y (2017) A clinical cassette dosing study for evaluating the contribution of hepatic OATPs and CYP3A to drug-drug interactions. *Pharm Res* **34**:1570–1583.
Zamek-Gliszczynski MJ, Lee CA, Poirier A, Bentz J, Chu X, Ellens H, Ishikawa T, Jamei M, Kalvass JC, Nagar S, et al. (2013) ITC recommendations for transporter kinetic parameter estimation and translational modeling of transport-mediated PK and DDIs in humans. *Clin Pharmacol Ther* **94**:64–79.

Address correspondence to: Dr. Aleksandra Galetin, Centre for Applied Pharmacokinetic Research, School of Health Sciences, University of Manchester, Stopford Building, Oxford Road, M13 9PT Manchester, UK. E-mail: Aleksandra.Galetin@manchester.ac.uk

Downloaded from jpet.aspetjournals.org at ASPET Journals on April 19, 2024

Supplementary Material for the manuscript: "In vitro – in vivo extrapolation of OATP1B-mediated drug-drug interactions in cynomolgus monkey"

A. Ufuk, R. E. Kosa, H. Gao, YA. Bi, S. Modi, D. Gates, A. D. Rodrigues, L. M. Tremaine , M. V. S. Varma, J. B. Houston and A. Galetin

Centre for Applied Pharmacokinetic Research, School of Medicine, Biology and Health Sciences, University of Manchester, UK (AU, JBH and AG)

Pharmacokinetics, Dynamics and Metabolism, Medicine Design, Pfizer Worldwide R&D, Groton, CT (REK, HG, YAB, ADR, LMT and MVSV)

Research Formulations, Pharmaceutical Sciences, Medicine Design, Pfizer Worldwide R&D, Groton, CT (SM and DG)

1. ***In vitro*** **sample preparation and LC-MS/MS analysis.** All samples were thawed and quenched with equal volume of methanol containing internal standard (IS). Naloxone (0.1 µM) and atorvastatin (0.5 µM) were the internal standards for rosuvastatin and pitavastatin, respectively. Both IS solutions were also used in the analysis of rifampicin and cyclosporine. Following quenching with IS/MeOH, samples were placed at -20°C for at least an hour to precipitate the proteins, followed by their centrifugation at 2500 rpm for 10 minutes (Eppendorf Centrifuge 5804, Cambridge, UK). The 20 µL of supernatant was analysed by LC-MS/MS. The analysis was performed on a Waters Alliance 2795 HPLC system coupled to a Micromass Quattro Ultima mass spectrometer (Waters, Watford, UK) using electrospray positive ionisation mode. The analytes and their internal standards were separated on Luna C18 column (3 µm, 50 x 4.6 mm) (Phenomenex, Macclesfield, UK). The mobile phases used were: Solvent A, 90% water, 10% methanol, and 0.05% formic acid; Solvent B, 10% water, 90% methanol, and 0.05% formic acid; Solvent C, 90% water, 10% methanol, and 1 mM ammonium acetate; and Solvent D, 10% water, 90% methanol, and 1 mM ammonium acetate. The gradient of mobile phases varied for each drug. The flow rate through HPLC was 1 mL/min, which was then split to 0.25 mL/min before entry into the mass spectrometer. For the Waters Ultima, the capillary voltage was 3.5 kV; desolvation and source temperatures were 350 and 125°C, respectively; desolvation gas and cone gas flow rates were 600 and 150 L/hr, respectively.

2. Analysis of $^{2}H_4$-pitavastatin, $^{2}H_6$-rosuvastatin, pitavastatin, rosuvastatin and rifampicin. The concentrations of these drugs were measured in plasma samples treated with 0.1 M sodium acetate buffer (pH 4) using the LC-MS/MS system listed above. All standards and QCs were made in blank monkey plasma mixed with an equal volume of 0.1 M sodium acetate buffer (pH 4). Standard and QC mixtures of the analytes were made to encompass a range of concentrations (0.1 to 500 ng/ml, $^{2}H_4$-pitavastatin; 1 to 5,000 ng/ml, rifampicin). Samples were diluted to be measured in the linear range of the instrument responses; with the high specificity of MRM (no interference in the blank matrixes) and a wide dynamic range for each analyte, the dilution integrity was confirmed by independent analysis of the drugs in the samples in separate assays. Aliquots of 50 µl of standards, QCs and plasma samples were prepared by protein precipitation using 200 µl of acetonitrile containing an internal standard mixture of simvastatin and $^{2}H_8$-rifampicin (100 ng/ml). The plates were vortexed for 2 minutes, centrifuged at 3000 rpm for 10 minutes, and 100 µl supernatants of the mixture were transferred for LC-MS/MS analysis. Chromatographic separation was accomplished on a Waters Acquity UPLC HSS T3 C18 column (1.8µm, 2.1 × 50 mm) maintained at 40 °C. The mobile phase consisted of two solvents, solvent A (0.1% formic acid in water) and solvent B (0.1% formic acid in acetonitrile). The total run time for each injection was 3 minutes. The flow rate was 0.6 ml/min. The gradient was maintained at 5% B for 0.3 min, followed by a linear increase to 95% B in 1.8 minutes, and kept at 95% B for 0.3 min then a linear decrease to 5% in 0.3 minutes. The column was equilibrated at 5% B for 0.3 min. A Valco VICI valve (Valco Instruments Co., Houston, TX) was used to divert the first 0.3 min and the last 0.5 minutes of HPLC effluent to waste. The injection volume was 2 µl.

References

Amundsen R, Christensen H, Zabihyan B and Asberg A (2010) Cyclosporine A, but not tacrolimus, shows relevant inhibition of organic anion-transporting protein 1B1-mediated transport of atorvastatin. *Drug Metab Dispos* **38:**1499-1504.

Chu X, Shih SJ, Shaw R, Hentze H, Chan GH, Owens K, Wang S, Cai X, Newton D, Castro-Perez J, Salituro G, Palamanda J, Fernandis A, Ng CK, Liaw A, Savage MJ and Evers R (2015) Evaluation of cynomolgus monkeys for the identification of endogenous biomarkers for hepatic transporter inhibition and as a translatable model to predict pharmacokinetic interactions with statins in humans. *Drug Metab Dispos* **43:**851-863.

Gertz M, Cartwright CM, Hobbs MJ, Kenworthy KE, Rowland M, Houston JB and Galetin A (2013) Cyclosporine inhibition of hepatic and intestinal CYP3A4, uptake and efflux transporters: application of PBPK modeling in the assessment of drug-drug interaction potential. *Pharm Res* **30:**761-780.

Hasunuma T, Nakamura M, Yachi T, Arisawa N, Fukushima K, Iijima H and Saito Y (2003) The drug-drug interactions of pitavastatin (NK -104), a novel HMG -CoA reductase inhibitor and cyclosporine. *J Clin Ther Med* **19:**381-389.

He YJ, Zhang W, Chen Y, Guo D, Tu JH, Xu LY, Tan ZR, Chen BL, Li Z, Zhou G, Yu BN, Kirchheiner J and Zhou HH (2009) Rifampicin alte rs atorvastatin plasma concentration on the basis of SLCO1B1 521T>C polymorphism. *Clin Chim Acta* **405:**49-52.

Izumi S, Nozaki Y, Maeda K, Komori T, Takenaka O, Kusuhara H and Sugiyama Y (2015) Investigation of the impact of substrate selection on in vitro organic anion transporting polypeptide 1B1 inhibition profiles for the prediction of drug-drug interactions. *Drug Metab Dispos* **43:**235-247.

Lau YY, Huang Y, Frassetto L and Benet LZ (2007) effect of OATP1B transporter inhibition on the pharmacokinetics of atorvastatin in healthy volunteers. *Clin Pharmacol Ther* **81:**194-204.

Maeda K, Ikeda Y, Fujita T, Yoshida K, Azuma Y, Haruyama Y, Yamane N, Kumagai Y and Sugiyama Y (2011) Identification of the rate -determining process in the hepatic clearance of atorvastatin in a clinical cassette microdosing study. *Clin Pharmacol Ther* **90:**575-581.

Pahwa S, Alam K, Crowe A, Farasyn T, Neuhoff S, Hatley O, Ding K and Yue W (2017) Pretreatment With Rifampicin and Tyrosine Kinase Inhibitor Dasatinib Potentiates the Inhibitory Effects Toward OATP1B1- and OATP1B3-Mediated Transport. *J Pharm Sci* **106:**2123-2135.

Prueksaritanont T, Chu X, Evers R, Klopfer SO, Caro L, Kothare PA, Dempsey C, Rasmussen S, Houle R, Chan G, Cai X, Valesky R, Fraser IP and Stoch SA (2014) Pitavastatin is a more sensitive and selective organic anion-transporting polypeptide 1B clinical probe than rosuvastatin. *Br J Clin Pharmacol* **78:**587-598.

Shen H, Su H, Liu T, Yao M, Mintier G, Li L, Fancher RM, Iyer R, Marathe P, Lai Y and Rodrigues AD (2015) Evaluation of rosuvastatin as an organic anion transporting polypeptide (OATP) probe substrate: in vitro transport and in vivo disposition in cynomolgus monkeys. *J Pharmacol Exp Ther* **353:**380-391.

Shen H, Yang Z, Mintier G, Han YH, Chen C, Balimane P, Jemal M, Zhao W, Zhang R, Kallipatti S, Selvam S, Sukrutharaj S, Krishnamurthy P, Marathe P and Rodrigues AD (2013) Cynomolgus monkey as a potential model to assess drug interactions involving hepatic organic anion transporting polypeptides: in vitro, in vivo, and in vitro-to-in vivo extrapolation. *J Pharmacol Exp Ther* **344:**673-685.

Simonson SG, Raza A, Martin PD, Mitchell PD, Jarcho JA, Brown CD, Windass AS and Schneck DW (2004) Rosuvastatin pharmacokinetics in heart transplant recipients administered an antirejection regimen including cyclosporine. *Clin Pharmacol Ther* **76:**167-177.

Takahashi T, Ohtsuka T, Uno Y, Utoh M, Yamazaki H and Kume T (2016) Pre -incubation with cyclosporine A potentiates its inhibitory effects on pitavastatin uptake mediated by recombinantly expressed cynomolgus monkey hepatic organic anion transporting polypeptide. *Biopharm Drug Dispos* **37:**479-490.

Takahashi T, Ohtsuka T, Yoshikawa T, Tatekawa I, Uno Y, Utoh M, Yamazaki H and Kume T (2013) Pitavastatin as an in vivo probe for studying hepatic organic anion transporting polypeptide-mediated drug-drug interactions in cynomolgus monkeys. *Drug Metab Dispos* **41:**1875-1882.

Thakare R, Gao H, Kosa RE, Bi YA, Varma MVS, Cerny MA, Sharma R, Kuhn M, Huang B, Liu Y, Yu A, Walker GS, Niosi M, Tremaine L, Alnouti Y and Rodrigues AD (2017) Leveraging of

Rifampicin-Dosed Cynomolgus Monkeys to Identify Bile Acid 3-O-Sulfate Conjugates as Potential Novel Biomarkers for Organic Anion-Transporting Polypeptides. *Drug Metab Dispos* **45:**721-733.

Watanabe M, Watanabe T, Yabuki M and Tamai I (2015) Dehydroepiandrosterone sulfate, a useful endogenous probe for evaluation of drug-drug interaction on hepatic organic anion transporting polypeptide (OATP) in cynomolgus monkeys. *Drug Metab Pharmacokinet* **30:**198-204.

Table S1

In vivo drug-drug interactions reported for OATP probe substrates in cynomolgus monkeys and humans

Cynomolgus monkey							Human						
Victim	Victim Route	Victim Dose (mg/kg)	Perpetrator	Route	Dose (mg/kg)	AUCR	Victim Route	Victim Dose (mg)	Perpetrator	Route	Dose (mg)	AUCR	Ref
Rosuvastatin	oral	3	CsA	oral	100	6.3	oral	10	CsA	oral	75-200	7.1 [a]	1, 2
(Class 3B)	oral	3	Rifampicin	oral	18	4.85	oral	5	Rifampicin	oral	600	4.37	3, 4
	i.v.	1	Rifampicin	oral	18	2.66	oral	5	Rifampicin	i.v.	600	1.32	3, 4
	oral	3	Rifampicin	oral	15	2.89							5
	oral	1	Rifampicin	oral	2	3 [a]							6
	oral	1	Rifampicin	oral	10	13.8 [a]							6
Pitavastatin	oral	0.3	CsA	oral	75	10.6	oral	2	CsA	oral	131	4.6	7, 8
	i.v.	0.3	CsA	oral		3.38							7
(Class 1B)	oral	1	Rifampicin	oral	2	3.35 [a]	oral	1	Rifampicin	oral	600	5.7	4, 6
							oral	1	Rifampicin	i.v.	600	0.75	4
	oral	1	Rifampicin	oral	10	10.2 [a]							6
	oral	0.3	Rifampicin	oral	20	14.8							7
	i.v.	0.3	Rifampicin	oral	20	3.83							7
	i.v.	0.2	Rifampicin	oral	1	1.2 [a]							9
	i.v.	0.2	Rifampicin	oral	3	2.4 [a]							
	i.v.	0.2	Rifampicin	oral	10	3.8 [a]							
	i.v.	0.2	Rifampicin	oral	30	4.5 [a]							
Atorvastatin	oral	1	Rifampicin	oral	2	2.32 [a]	oral	2.5	Rifampicin	oral	600	12 [a]	6, 10
(Class 1B)	oral	1	Rifampicin	oral	10	11.8 [a]	oral	40	Rifampicin	oral	600	8.5 [b]	6, 11
	oral	5	Rifampicin	oral	18	1.67	oral	40	Rifampicin	i.v.	600	7.8	3, 12
	i.v.	1	Rifampicin	oral	18	1.65							

[a] *$AUC_{0\text{-}last}$;* [b] *AUCR of OATP1B1 521TT group cited*

References: [1] Simonson et al. (2004); [2] Shen et al. (2015); [3] Chu et al. (2015); [4] Prueksaritanont et al. (2014); [5] Shen et al. (2013); [6] Watanabe et al. (2015); [7] Takahashi et al. (2013); [8] Hasunuma et al. (2003); [9] Thakare et al. (2017); [10] Maeda et al. (2011); [11] He et al. (2009); [12] Lau et al. (2007)

Table S2

LC-MS/MS conditions used for the analysis of rosuvastatin, pitavastatin, rifampicin, cyclosporine A and rifampicin SV in cynomolgus monkey hepatocytes

Internal standard used when analysed with [1] pitavastatin and [2] rosuvastatin; LLOQ: lower limit of quantification

Compound	Mass transition (m/z)	Cone voltage (V)	Collision voltage (eV)	Retention time (min)	LLOQ (µM)	Internal Standard	Mass transition (m/z)	Cone voltage (V)	Collision voltage (eV)	Retention time (min)
Rosuvastatin	482.3>258.2	60	30	3.90	0.01	Naloxone	328.15>310.05	80	20	3.15
Pitavastatin	422.15>290.25	40	25	3.40	0.01	Atorvastatin	559.25>440.4	60	21	3.70
Rifampicin	823.6>791.4	60	15	3.06	0.01	Atorvastatin [1]	559.25>440.4	60	21	3.70
	823.6>791.4	60	15	4.38	0.01	Naloxone [2]	328.15>310.05	80	20	3.15
Cyclosporine A	1225.05>1112.75	150	65	5.30	0.10	Atorvastatin [1]	559.25>440.4	60	21	3.70
	1225.05>1112.75	150	65	5.73	0.10	Naloxone [2]	328.15>310.05	80	20	3.15
Rifamycin SV	696.15>272.2	50	35	5.20	0.1	Tolbutamine	269.00>170.00	75	17	4.50

Table S3

LC-MS/MS conditions used for the analysis of $^{2}H_4$-pitavastatin, $^{2}H_6$-rosuvastatin, pitavastatin, rosuvastatin and rifampicin

Compound	Q1 Mass (Da)	Q3 Mass (Da)	Dwell time (msec)	DP (eV)	CE (V)
Rosuvastatin	482.2	258.2	10	100	40
$^{2}H_6$-Rosuvastatin	488.2	264.2	10	100	40
Rosuvastatin lactone	464.2	271.2	10	100	40
Pitavastatin	422.2	290.2	10	100	40
$^{2}H_4$-Pitavastatin	426.2	294.2	10	100	40
Pitavastatin lactone	404.2	290.2	10	100	40
Rifampicin	823.4	791.7	10	100	17
$^{2}H_8$-rifampicin	831.4	799.7	10	100	17
Simvastatin	419.2	285.2	10	80	15

Table S4

IC_{50} of cyclosporine and rifampicin on the OATP1B1 and OATP1B3-mediated uptake of clinical and non-clinical probe substrates with or without pre-incubation in HEK293 cells expressing human and monkey OATPs (hOATPs and cOATPs, respectively)

Inhibitor	Substrate	System	IC_{50} (μM)		Fold change	Reference
			Pre-incubation with buffer	Pre-incubation with inhibitor		
Cyclosprine A	Estradiol glucuronide	HEK293-hOATP1B1	0.198 ± 0.017	0.019 ± 0.007	10.4	Gertz et al. (2013)
	Estradiol glucuronide	HEK293-hOATP1B3	0.162 ± 0.056	0.032 ± 0.003	5.10	Gertz et al. (2013)
	Atorvastatin	HEK293-hOATP1B1	0.470 ± 0.340	0.021 ± 0.004	22.0	Amundsen et al. (2010)
	Pitavastatin	HEK293-hOATP1B1	0.102 ± 0.037	0.026 ± 0.004	3.90	Izumi et al. (2015)
	Atorvastatin	HEK293-hOATP1B1	0.112 ± 0.028	0.026 ± 0.004	4.31	Izumi et al. (2015)
	Sulfobromophthalein	HEK293-hOATP1B1	0.252 ± 0.057	0.080 ± 0.027	3.15	Izumi et al. (2015)
	Estrone-2-sulfate	HEK293-hOATP1B1	0.134 ± 0.017	0.026 ± 0.009	5.15	Izumi et al. (2015)
	Estradiol-17β-glucuronide	HEK293-hOATP1B1	0.046 ± 0.004	0.014 ± 0.007	3.29	Izumi et al. (2015)
	Pitavastatin	HEK293-cOATP1B1	0.620 ± 0.090	0.027 ± 0.011	23.0	Takahashi et al. (2016)
	Pitavastatin	HEK293-cOATP1B3	0.850 ± 0.210	0.110 ± 0.030	7.73	Takahashi et al. (2016)
Rifampicin	Pitavastatin	HEK293-cOATP1B1	1.20 ± 0.50	0.68 ± 0.25	1.76	Takahashi et al. (2016)
	Pitavastatin	HEK293-cOATP1B3	7.60 ± 3.20	8.90 ± 1.10	0.85	Takahashi et al. (2016)
	Estradiol-17β-glucuronide	HEK293-hOATP1B1	0.740 ± 0.08	0.24 ± 0.03	3.10	Pahwa et al. (2017)
	Estradiol-17β-glucuronide	HEK293-hOATP1B3	0.26 ± 0.03	0.11 ± 0.01	2.36	Pahwa et al. (2017)

Table S5

Plasma area under the curve (AUC) values of rosuvastatin and pitavastatin lactone in the absence and presence of oral rifampicin (1-30 mg/kg) after oral administration of rosuvastatin and pitavastatin (2 mg/kg)

		PK Parameter	Individual PK Parameters					
			Subject 13-310	Subject 13-445	Subject 13-462	Subject 14-1812	Mean	SD
Rosuvastatin Lactone	Control	$AUC_{0-\infty}$ (ng.h/mL)	131 (1)	220 (1)	142 (1)	136 (1)	157.3 (1)	42 (0)
	+RIF 1 mg/kg	$AUC_{0-\infty}$ (ng.h/mL)	442 (3.4)	901 (4.1)	406 (2.9)	349 (2.6)	524.5 (3.3)	254 (0.7)
	+RIF 3 mg/kg	$AUC_{0-\infty}$ (ng.h/mL)	463 (3.5)	515 (2.3)	191 (1.3)	202 (1.5)	342.8 (2.2)	170 (1.0)
	+RIF 10 mg/kg	$AUC_{0-\infty}$ (ng.h/mL)	250 (1.9)	512 (2.3)	252 (1.8)	264 (1.9)	319.5 (2.0)	128 (0.2)
	+RIF 30 mg/kg	$AUC_{0-\infty}$ (ng.h/mL)	223 (1.7)	566 (2.6)	321 (2.3)	296 (2.2)	351.5 (2.2)	149 (0.4)
Pitavastatin Lactone	Control	$AUC_{0-\infty}$ (ng.h/mL)	13.1 (1)	148 (1)	50.1 (1)	64.4 (1)	68.9 (1)	57 (0)
	+RIF 1 mg/kg	$AUC_{0-\infty}$ (ng.h/mL)	87.9 (6.7)	432 (2.9)	136 (2.7)	259 (4.0)	229 (4.1)	153 (1.8)
	+RIF 3 mg/kg	$AUC_{0-\infty}$ (ng.h/mL)	1050 (80.2)	1520 (10.3)	394 (7.9)	480 (7.5)	861 (26.5)*	527 (35.8)
	+RIF 10 mg/kg	$AUC_{0-\infty}$ (ng.h/mL)	219 (16.7)	575 (3.9)	239 (4.8)	253 (3.9)	322 (7.3)	170 (6.3)
	+RIF 30 mg/kg	$AUC_{0-\infty}$ (ng.h/mL)	321 (24.5)	1230 (8.3)	548 (10.9)	306 (4.8)	601 (12.1)	434 (8.6)

The numbers in brackets indicate the AUC ratios relative to control in individual animals, and the mean and standard deviation (SD) of the AUC ratios observed in all animals. *One-way ANOVA with Dunnett's multiple comparisons test was employed to test significance with *p<0.05*

Table S6

Plasma area under the curve (AUC) of the lactone to acid ratio of oral rosuvastatin and pitavastatin (2 mg/kg) in the absence and presence of rifampicin (1-30 mg/kg)

		PK Parameter	Individual PK Parameters					
			Subject 13-310	Subject 13-445	Subject 13-462	Subject 14-1812	Mean	SD
Rosuvastatin	Control	$AUC_{lactone}$:AUC_{acid}	3.47	3.75	3.59	2.17	3.25	0.73
	+RIF 1 mg/kg	$AUC_{lactone}$:AUC_{acid}	10.1	11.7	11.2	3.59	9.14**	3.76
	+RIF 10 mg/kg	$AUC_{lactone}$:AUC_{acid}	0.85	1.43	0.72	0.30	0.83	0.46
	+RIF 30 mg/kg	$AUC_{lactone}$:AUC_{acid}	0.62	0.86	0.69	0.20	0.59	0.28
Pitavastatin	Control	$AUC_{lactone}$:AUC_{acid}	0.10	0.37	0.23	0.15	0.21	0.12
	+RIF 1 mg/kg	$AUC_{lactone}$:AUC_{acid}	0.32	1.04	0.56	0.23	0.54	0.36
	+RIF 10 mg/kg	$AUC_{lactone}$:AUC_{acid}	0.11	0.34	0.11	0.02	0.15	0.14
	+RIF 30 mg/kg	$AUC_{lactone}$:AUC_{acid}	0.13	0.25	0.17	0.02	0.14	0.09

*One-way ANOVA with Dunnett's multiple comparisons test was employed to test significance with **p<0.01*

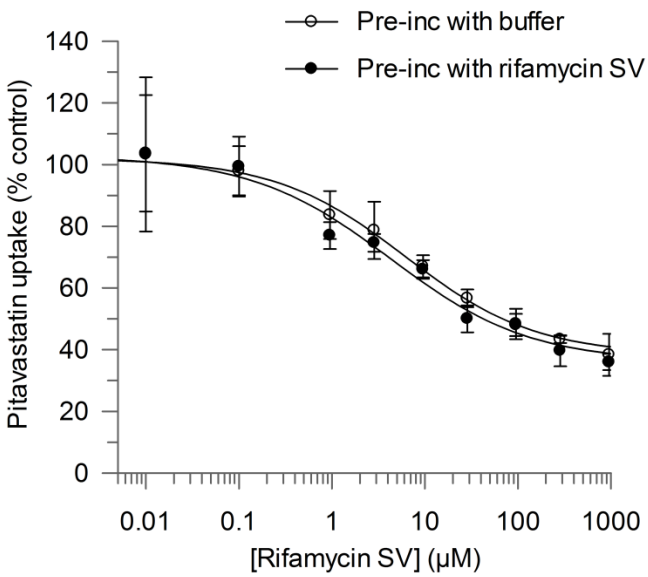

Figure S1. Rifamycin SV concentration-dependent inhibition of pitavastatin in cryopreserved cynomolgus monkey hepatocytes plated for 4h. Pre-incubation with either buffer or rifamycin SV (0.01-1000 µM) was performed for 1h prior to co-incubation with rifamycin SV and pitavastatin. Data represent mean ± SD of triplicate measurements.